

Supplementary Information

Aufbau vs. Non-Aufbau Ground States in Two-Coordinate d^7 Single-Molecule Magnets

Dylan Errulat,^{a‡} Katie L. M. Harriman,^{a‡} Diogo A. Gálico,^a Jeffrey S. Ovens,^a Akseli Mansikkamäki ^{b*} and Muralee Murugesu ^{a*}

^a Department of Chemistry and Biomolecular Sciences, University of Ottawa, Ottawa, Ontario K1N 6N5, Canada.

^b NMR Research Unit, University of Oulu, P. O. Box 3000, 90014 Oulu, Finland.

*Corresponding Authors: M. Murugesu (E-mail: m.murugesu@uottawa.ca) and A. Mansikkamäki (akseli.mansikkamaki@oulu.fi)

‡ These authors contributed equally to this work.

Table of Contents

Materials and Methods.....	S2
X-Ray Crystallographic Details	S4
Details of <i>Ab Initio</i> Calculations.....	S7
Magnetic Measurement Details and Additional Plots.....	S16
Magnetic Circular Dichroism Details.....	S44
References	S48

Materials and Methods

All operations were performed in a M. Braun glovebox under an atmosphere of purified dinitrogen or using high vacuum standard Schlenk techniques. Solvents were dried using a J.C. Meyer solvent system, degassed with successive free-pump-thaw cycles, and stored over activated 4 Å molecular sieves. FeCl₂ and CoCl₂ were purchased from Strem Chemicals in anhydrous form at 98 % and 99+% purity, respectively. 2,2,2-Cryptand was purchased from Sigma Aldrich and used without prior purification. Potassium metal was purchased from Alfa Aesar, which were washed with aliquots of hexanes to remove the mineral oil used for storage and the oxide coating was removed prior to use. Benzene-*d*₆ was purchased from Cambridge Isotope Laboratories, degassed with successive free-pump-thaw cycles and dried over activated 4 Å molecular sieves for 48 h prior to use. Celite used for filtration was dried under vacuum while heating to 180 °C for 5 days. [K{N(SiMePh₂)₂}THF]_n was prepared according to literature procedure.¹ [Fe{N(SiMePh₂)₂}₂] and [Co{N(SiMePh₂)₂}₂] were synthesized following a previously published procedure with modifications detailed below.² All NMR data reported were measured using a Bruker AVANCE II 300 MHz spectrometer, and the ¹H NMR spectra were referenced to the residual solvent signal. FT-IR spectra were recorded on a Nicolet Nexus 550 FT-IR spectrometer using transmission mode in the 4000-600 cm⁻¹ range; solid samples were prepared in an inert atmosphere and sandwiched between transparent NaCl plates which were corrected for. Elemental Analyses were performed by Midwest Microlab.

Synthesis of [Co{N(SiMePh₂)₂}₂] (1). In a 20 mL scintillation vial, a solution of [K{N(SiMePh₂)₂}THF]_n (200 mg, 0.385 mmol) in diethyl ether (5 mL) was combined with a slurry of CoCl₂ (25 mg, 0.192 mmol) in diethyl ether (5 mL). The reaction proceeded at room temperature for 16 h. The solvent was removed from the reaction mixture under reduced pressure, yielding a dark green tacky solid. The product was extracted into toluene (4 mL) and filtered through a pad of Celite supported on a fine glass frit to remove KCl. The filtrate was collected, and equal parts n-hexanes were added. Dark green crystals of **1** were grown from storage of the n-hexanes/toluene solution at -35°C for 2 days. Isolated X-ray diffraction quality crystals are air and moisture sensitive. Yield: 105 mg, 63%. IR (neat, cm⁻¹): 2917 (w), 2850 (w), 1583 (w), 1482 (w), 1424 (m), 1308 (w), 1246 (w), 1162 (w), 1103 (m), 1029 (w), 1002 (m), 970 (m), 925 (w), 855 (w), 801 (m), 774 (w), 756 (w), 735 (m), 698 (m), 662 (w), 455 (s). ¹H NMR (25°C, 300 MHz, benzene-*d*₆): δ -50.4 (br s; *o*-*Ph*), -19.7 (br s, *m*-*Ph*), -15.9 (br s, *p*-*Ph*), 51.9 (br s, *Me*). Anal. Calcd for

$C_{52}H_{52}CoN_2Si_4$: C, 71.29; H, 5.99; N, 3.20. Found: C, 70.59; H, 6.10; N, 3.26.

Synthesis of $[Fe\{N(SiMePh_2)_2\}_2]$ (2). In a 20 mL scintillation vial, a solution of $[K\{N(SiMePh_2)_2\}THF]_n$ (200 mg, 0.385 mmol) in diethyl ether (5 mL) was combined with a slurry of $FeCl_2$ (24 mg, 0.192 mmol) in diethyl ether (5 mL). The reaction proceeded at room temperature for 16 h. The solvent was removed from the reaction mixture under reduced pressure, yielding a beige tacky solid. The product was extracted into toluene (4 mL) and filtered through a pad of Celite supported on a fine glass frit to remove KCl. The filtrate was collected, and equal parts n-hexanes was added. Pale green crystals of **2** were grown from storage of the n-hexanes/toluene solution at -35°C for 2 days. Isolated X-ray diffraction quality crystals are air and moisture sensitive. Yield: 101 mg, 60%. IR (neat, cm^{-1}): 3128 (w), 3065 (w), 2955 (w), 2896 (w), 2850 (w), 2795 (w), 1957 (w), 1898 (w), 1822 (w), 1766 (w), 1726 (w), 1711 (w), 1692 (w), 1660 (w), 1585 (w), 1564 (w), 1551 (w), 1531 (w), 1484 (w), 1424 (m), 1380 (w), 1241 (m), 1189 (w), 1157 (w), 1130 (w), 1103 (s), 1029 (m), 971 (s), 801 (s), 777 (s), 731 (m), 699 (m), 662 (w), 447 (s). 1H NMR (25°C, 300 MHz, benzene- d_6): δ -30.3 (br s; *o-Ph*), -12.2 (br s; *m-Ph*), -10.2 (br s; *p-Ph*), 59.4 (br s; *Me*).

Synthesis of $[K(2,2,2\text{-crypt})][Fe\{N(SiMePh_2)_2\}_2]$ (3). In a 20 mL scintillation vial, a solution of **1-Fe** (127 mg, 0.14 mmol) in toluene (5 mL) was combined with 2,2,2-cryptand (55 mg, 0.14 mmol) in toluene (2 mL). This combined solution was added to a precooled (-35 °C) slurry of KC_8 (20 mg, 0.14 mmol) in toluene (10 mL). The reaction was stirred for 2 h gradually warming to room temperature. The dark purple solution was filtered through a plug of Celite supported on a fine glass frit. The plug was washed with 3 aliquots of 4 mL toluene and the filtrate collected. Reducing the filtrate volume by half and storage at room temperature resulted in the growth of dark purple crystals over two days. Isolated X-ray diffraction quality crystals are air and moisture sensitive. Yield: 32 mg, 18%. IR (neat, cm^{-1}): 3415 (br), 3060 (w), 2919 (w), 2851 (w), 1584 (w), 1483 (w), 1443 (w), 1423 (w), 1353 (w), 1323 (w), 1293 (w), 1257 (w), 1235 (w), 1171 (w), 1131 (w), 1103 (m), 1052 (w), 1021 (w), 984 (w), 948 (w), 925 (w), 856 (w), 805 (w), 778 (w), 732 (w), 698 (m), 456 (s). 1H NMR (25°C, 300 MHz, benzene- d_6): δ -12.2 (br s; *m-Ph*), -10.3 (br s; *p-Ph*), -5.8 (br s; *o-Ph*), -1.62, -1.26, and -1.01 (overlapping br s; *crypt*), 58.1 (br, s; *Me*). Anal. Calcd for $C_{70}H_{88}FeKN_4O_6Si_4$: C, 65.24; H, 6.89; N, 4.35. Found: C, 65.03; H, 6.85; N, 4.43.

X-ray Crystallographic Details

Data collection for the single crystals studied here (Table S1) were obtained on a Bruker SMART APEX diffractometer either at the University of Ottawa (**1**) or the Université de Montréal (**3**). A single crystal of **1** was mounted on a glass fiber and data was collected at 200 K. A suitable crystal of **3** was mounted on a cryoloop and the crystal was kept at 100 K during data collection. Absorption corrections were applied by using semi-empirical method of the SADABS program for all samples. The structures were solved by SHELXT³ and refined by full matrix least-squares methods on F² with SHELXL.⁴ Systematic absences in the diffraction data-set and unit cell parameters were consistent with monoclinic P2¹/c (No. 14) for **1** and monoclinic C2/c (No. 15) for compound **3**. For all compounds, all hydrogen atom positions were calculated based on the geometry of related non-hydrogen atoms. All hydrogen atoms were treated as idealized contributions during the refinement. It should be noted that the crystal structure for **1** was initially reported by Power and co-workers (CCDC: 577296),² however our studies have yielded a new solid state structure of the compound, and as such the structural details are included here. CCDC 2005382 (**1**) and 2005381 (**3**) contain the supplementary crystallographic data for this paper. These data can be obtained free of charge from the Cambridge Crystallographic Data Center.

Phase purity of the sample was confirmed *via* powder X-ray diffraction, performed on a RIGAKU Ultima IV diffractometer, equipped with a Cu-K α radiation source ($\lambda = 1.541836 \text{ \AA}$), and a graphite monochromator. Scanning of the 2θ range was performed from 5-38°. XRPD patterns were consistent in 2θ values with the generated pattern from SCXRD, with slight discrepancies in some intensities of the peaks, which is attributed to preferential orientation.

Table S1. Crystallographic Data for **1** and **3**.

	1 (Co ^{II})	3 (Fe ^I)
Empirical formula	C ₅₂ H ₅₂ CoN ₂ Si ₄	C ₇₀ H ₈₈ FeKN ₄ O ₆ Si ₄
Formula weight	876.25	1288.75
Temperature/K	200	100
Crystal system	Monoclinic	Monoclinic
Space group	P2 ₁ /c	C2/c
a/Å	16.1285(8)	21.2364(5)
b/Å	10.5317(5)	16.7283(4)
c/Å	27.5095(13)	19.7697(5)
α/°	90	90
β/°	100.973(2)	94.2480(10)
γ/°	90	90
Volume/ Å ³	4587.35	7003.93
Z	4	4
ρ _{calc} g/cm ³	1.269	1.222
μ/mm ⁻¹	0.516	3.321
F(000)	1844	2740.0
Crystal size/mm ³	0.105 x 0.063 x 0.015	0.3 x 0.25 x 0.05
Radiation	MoKα (λ= 0.71073)	CuKα(λ= 1.54178)
2θ range for data collection/°	1.286 to 26.408	6.734 to 144.384
Index ranges	-17 ≤ h ≤ 20 -13 ≤ k ≤ 13 -34 ≤ l ≤ 32	-26 ≤ h ≤ 25 -20 ≤ k ≤ 20 -24 ≤ l ≤ 24
Reflections collected	35978	62066
Independent reflections	9393 [R _{int} = 0.0783, R _{sigma} = 0.0933]	6882 [R _{int} = 0.0399, R _{sigma} = 0.0203]
Data/restraints/parameters	9393/0/536	6882/0/391
Goodness-of-fit on F ²	0.999	1.044
Final R indexes [I>=2σ(I)]	R ₁ = 0.0503, wR ₂ = 0.0918	R ₁ = 0.0359, wR ₂ = 0.0997
Final R indexes [all data]	R ₁ = 0.1127, wR ₂ = 0.1103	R ₁ = 0.0373, wR ₂ = 0.1013
Largest diff. peak/hole / e Å ⁻³	0.371/-0.35	0.85/-0.27

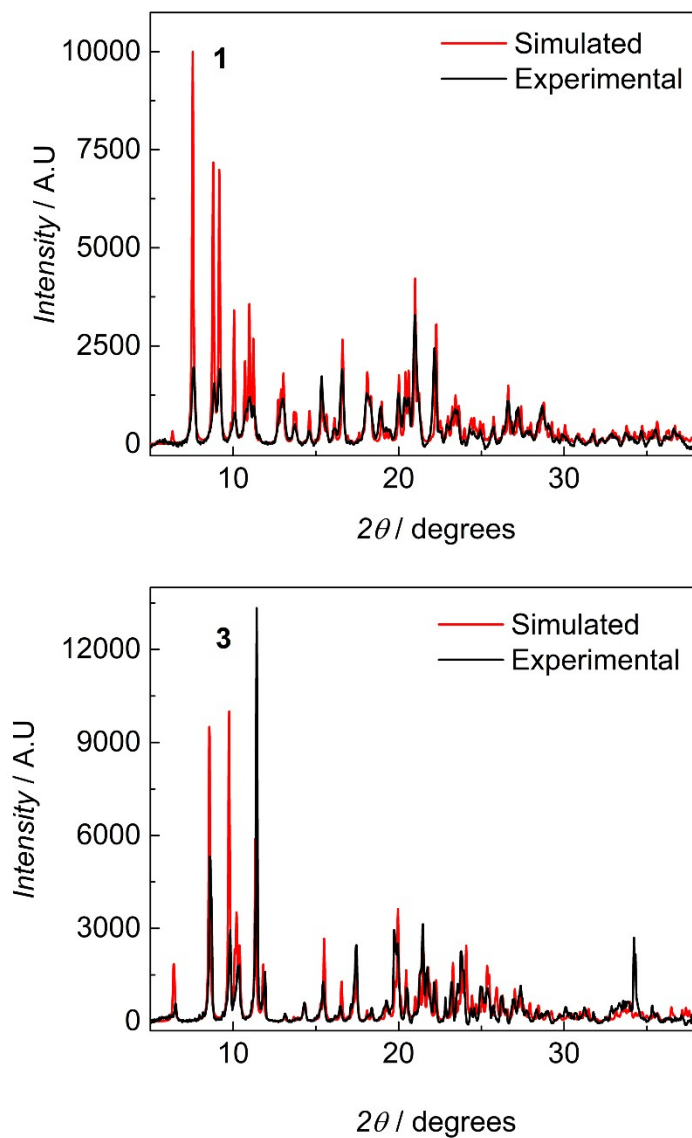


Fig. S1. Simulated (red) and the experimentally obtained (blue) powder X-ray diffraction pattern for **1** and **3**.

Details of *Ab Initio* Calculations

The geometries of **1** and **3** were extracted from the respective crystal structures. The positions of hydrogen atoms were optimized using density functional theory (DFT) level while the position of heavier atoms were kept frozen to the crystal-structure coordinates. The structures $[\text{Fe}\{\text{N}(\text{SiMe}_3)_2\}_2]^+$ and $\text{Co}\{\{\text{SiMe}_3\}_2\}_2$ used in the potential energy scans were optimized at DFT level. Constraints were placed on either the N–M–N angle or the Si–N–N–Si dehedral as well as the point group symmetry of the molecule. The DFT calculations on **1** and **3** were carried out using the *Gaussian 09* software revision E.01.⁸ The PBE0 hybrid exchange-correlation functional^{9,10} was used along with def2-SVP basis sets.¹¹ The integration grid was raised to “UltraFine” quality and the accuracy of the two-electron integrals was set to 10^{-12} atomic units. The constrained optimizations of the $[\text{Fe}\{\text{N}(\text{SiMe}_3)_2\}_2]^+$ and $\text{Co}\{\{\text{SiMe}_3\}_2\}_2$ structures were carried out using the *ADF 2019* code version 1.03.¹² The pure PBE exchange-correlation functional⁹ was used and scalar relativistic effects were introduced using the zeroth-order regular approximation (ZORA).¹³ Slater-type-basis sets with frozen cores were used for all atoms.¹⁴ A polarized triple- ζ quality basis sets (TZP) were used for the metal ions and polarized double- ζ quality basis sets were used for the remaining atoms. The 1s shell was frozen for C and N, all shells up to 2p for Si and up to 3p for the metals. The geometry convergence thresholds were raised to 10^{-4} , 10^{-4} , 10^{-3} and 10^{-1} atomic units for energy, gradient, bond length and bond angles, respectively.

The multireference calculations were carried out using the *Orca* quantum chemistry code¹⁵ versions 4.2.0 and 4.2.1 for the **1** and **3** structures and the scans, respectively. First a state-averaged complete active space self-consistent field (SA-CASSCF) calculation¹⁶ was carried out on each system. The active space consisted of the five 3d orbitals and the seven 3d electrons in all systems. All possible roots were solved in a single state-averaged calculation for each system. Additional test calculations with a double-shell active space of seven electron and ten orbitals as well as with an augmented active space of 17 electrons in ten orbitals were carried out. However, increasing the active space did not lead to visible improvement in the results. This consisted of 10 quartets and 40 doublets. The electron correlation outside the active space was then accounted up to second order using the *N*-electron valence state perturbation theory (NEVTP2) in its strongly contracted formulation.¹⁷ Scalar relativistic effects were introduced in the one-particle operator using the standard second order Doulas-Kroll-Heß (DKH) transformation.¹⁸ Spin-orbit coupling (SOC) was

introduced using the quasi-degenerate perturbation theory (QDPT) formulation.¹⁹ The SOC operator was constructed in the basis of all SA-CASSCF eigenstates using the spin-orbit mean-field (SOMF) operator.²⁰ The NEVPT2 contribution to the SOC was included as a simple diagonal shift to the SOC operator, and the effect of the NEVPT2 correction on the off-diagonal elements of the SOC operator was not considered. The operator was then diagonalized to yield the final spin-orbit coupled states.

Basis sets of the DKH-def2 type were used throughout.²¹ These basis sets are re-contracted version of the def2 basis sets and specifically optimized for DKH calculations. In the case of **1** and **3**, double-polarized triple- ζ quality (DKH-def2-TZVPP) basis sets were used for the metal ions, polarized triple- ζ quality (DKH-def2-TZVP) basis sets were used for the N and Si atoms and polarized triple- ζ quality (DKH-def2-TZVP) basis sets were used for the H and C atoms. In the case of $[\text{Fe}\{\text{N}(\text{SiMe}_3)_2\}_2]^+$ and $\text{Co}\{(\text{SiMe}_3)_2\}_2$ DKH-def2-TZVP basis sets were used for the metal ions and polarized double- ζ quality (DKH-def2-SVP) basis sets were used for the remaining atoms. In all cases, the resolution of identity (RI) approximation was used in the integral transformations, and the necessary auxiliary basis set was generated using the “AutoAux” feature implemented in *Orca*.²²

The energies of the free-ion orbitals were evaluated from NEVPT2/CASSCF calculations at the same level of theory. The orbital energies of the $3d$ orbitals correspond to the diagonal elements of the generalized SA-CASSCF Fock operator, as the operator is not diagonal in the basis of the natural. The off-diagonal elements are, however, very small and the order of magnitudes are definitely correct. The *ab initio* ligand-field (AILFT) analysis was carried out using the method as implemented in Orca.²³

Table S2. Full results of the AILFT calculations including the AILFT orbital energies, the Racah parameters (A, B and C), the Slater–Condon parameters (F^0 , F^2 , F^4) and the spin-orbit coupling constant ζ . All values are in units cm^{-1} .

	1 (Co^{II})	3 (Fe^{I})
Orbital energies	0.0	0.0
	534.7	2506.3
	3005.8	2571.1
	5865.3	3593.1
	7906.3	5521.9
	187614.8	159718.2
<i>A</i>	965.1	723.9
<i>B</i>	3754.8	3165.1
<i>C</i>	192871.5	164149.4
F^0	73571.0	57626.0
F^2	47310.2	39880.7
ζ	507.1	342.0

Table S3. Reduced Löwdin composition of the active orbitals. The labels of the columns are the indices of the orbitals in the CASSCF calculations. (Note that while the shapes of the CASSCF and AILFT orbitals are the same, their energies are different; therefore, the ordering of the CASSCF orbitals is not the same as that of the AILFT orbitals.)

	1 (Co^{II})				
	227	228	229	230	231
$4s$	0.000	0.000	0.000	0.000	0.000
$3d_{z^2}$	0.000	0.000	0.961	0.000	0.001
$3d_{xy}$	0.938	0.000	0.000	0.000	0.000
$3d_{xz}$	0.000	0.000	0.000	0.964	0.001
$3d_{yz}$	0.000	0.988	0.000	0.000	0.000
$3d_{x^2-y^2}$	0.000	0.000	0.002	0.000	0.924
	3 (Fe^{I})				
	227	228	229	230	231
$4s$	0.000	0.000	0.029	0.000	0.106
$3d_{z^2}$	0.000	0.000	0.934	0.000	0.001
$3d_{xy}$	0.957	0.000	0.000	0.000	0.000
$3d_{xz}$	0.000	0.000	0.000	0.961	0.000
$3d_{yz}$	0.000	0.993	0.000	0.000	0.000
$3d_{x^2-y^2}$	0.000	0.000	0.015	0.000	0.797

Table S4. NEVPT2 energies.

State	1 (Co ^{II})		3 (Fe ^I)	
	2S + 1	E / cm ⁻¹	2S + 1	E / cm ⁻¹
1	4	0	4	0
2	4	382.6	4	266.6
3	4	3546.3	4	7719.9
4	4	4668.8	4	9085.7
5	4	4803.7	4	11686.4
6	4	4822.5	4	11737.9
7	4	6170.1	4	13171.4
8	4	13820.9	2	16569.5
9	2	14623.1	2	16582.5
10	2	16045	2	18007.5
11	2	16118.7	2	18112.9
12	2	16131.6	4	18183.5
13	2	16380.1	2	18243.7
14	2	18128.8	2	18559.7
15	2	18578.6	2	18780.5
16	2	18778.5	4	19702.9
17	2	19689	2	20327.9
18	2	19875.1	2	20832
19	2	19935.3	2	21823.6
20	4	20099.4	2	21827.6
21	2	20173.9	4	22346.3
22	2	20588.6	2	22741.5
23	2	21058	2	22849.2
24	4	22764.6	2	22882.5
25	2	23359.9	2	23879.9
26	2	23505.8	2	23890.2
27	2	24298	2	24354.6
28	2	24463.2	2	24368.4
29	2	24943	2	25006.5
30	2	24972.9	2	26518.1
31	2	25210.2	2	26775.2
32	2	26862.9	2	27261.2
33	2	27223.7	2	27806.1
34	2	27357.5	2	28935.6
35	2	28143.6	2	29482.1
36	2	28569.1	2	29666

37	2	31542.6	2	30475.9
38	2	31553.3	2	30506.5
39	2	36521.1	2	34420
40	2	36893.8	2	35130.6
41	2	38915.7	2	35425.3
42	2	39039.6	2	35551.6
43	2	39745.9	2	36672.5
44	2	40936.1	2	36698
45	2	40982.1	2	36792.9
46	2	53280	2	47631.4
47	2	56262.9	2	49889.7
48	2	56572.6	2	50306.1
49	2	64391.2	2	50765.8
50	2	64673.3	2	54092.5

Table S5. Eigenvalues of the SOC operator.

State		E / cm^{-1}	
	1 (Co ^{II})		3 (Fe ^I)
1	0		0
2	0		0
3	369.4		189.6
4	369.4		189.6
5	938.3		547.3
6	938.3		547.3
7	1323.1		762.1
8	1323.1		762.1
9	3822.4		7922.9
10	3822.4		7922.9
11	3929.3		7957.4
12	3929.3		7957.4
13	4632.4		9312.4
14	4632.4		9312.4
15	5033.8		9360
16	5033.8		9360
17	5168.6		11459.9
18	5168.6		11459.9
19	5329.9		11787.3

20	5329.9	11787.3
21	5614.9	12117.1
22	5614.9	12117.1
23	5919.1	12441.2
24	5919.1	12441.2
25	6824	13440.6
26	6824	13440.6
27	6972.2	13475.7
28	6972.2	13475.7
29	14266.5	16597.3
30	14266.5	16597.3
31	14300.8	17043.1
32	14300.8	17043.1
33	15021.6	18194
34	15021.6	18194
35	16133.1	18329.7
36	16133.1	18329.7
37	16630	18396.1
38	16630	18396.1
39	16906	18407.9
40	16906	18407.9
41	17099.9	18468
42	17099.9	18468
43	18513.8	18934.4
44	18513.8	18934.4
45	19139.1	19091.6
46	19139.1	19091.6
47	19296	19902.6
48	19296	19902.6
49	20112.2	19953.5
50	20112.2	19953.5
51	20353.9	20535.7
52	20353.9	20535.7
53	20407.8	21136.5
54	20407.8	21136.5
55	20510.5	21904.2
56	20510.5	21904.2
57	20681	22297
58	20681	22297
59	20839.6	22404.6
60	20839.6	22404.6

61	21295.3	22571
62	21295.3	22571
63	21740.4	22963.1
64	21740.4	22963.1
65	23117	23131.6
66	23117	23131.6
67	23249	23235.7
68	23249	23235.7
69	23789.5	24179.3
70	23789.5	24179.3
71	24125.3	24306.9
72	24125.3	24306.9
73	24657.7	24528.7
74	24657.7	24528.7
75	25199.6	24777.6
76	25199.6	24777.6
77	25439.3	25349.6
78	25439.3	25349.6
79	25709.1	26777.3
80	25709.1	26777.3
81	26069.4	27133.7
82	26069.4	27133.7
83	27363.9	27556.7
84	27363.9	27556.7
85	27660.7	28119.4
86	27660.7	28119.4
87	28135.3	29273.1
88	28135.3	29273.1
89	28605.5	29569.3
90	28605.5	29569.3
91	29522	30188.7
92	29522	30188.7
93	31844.4	30745.7
94	31844.4	30745.7
95	32401	30814.5
96	32401	30814.5
97	37038.8	34678.5
98	37038.8	34678.5
99	37444.2	35384.4
100	37444.2	35384.4
101	39410.2	35693.2

102	39410.2	35693.2
103	39618	35826.9
104	39618	35826.9
105	40305.6	36870.4
106	40305.6	36870.4
107	41346.4	37035.4
108	41346.4	37035.4
109	41685.7	37073.3
110	41685.7	37073.3
111	53857.3	47918
112	53857.3	47918
113	56737.5	50172.2
114	56737.5	50172.2
115	57249.2	50579.2
116	57249.2	50579.2
117	64779.4	51071.8
118	64779.4	51071.8
119	65416.2	54382.4
120	65416.2	54382.4

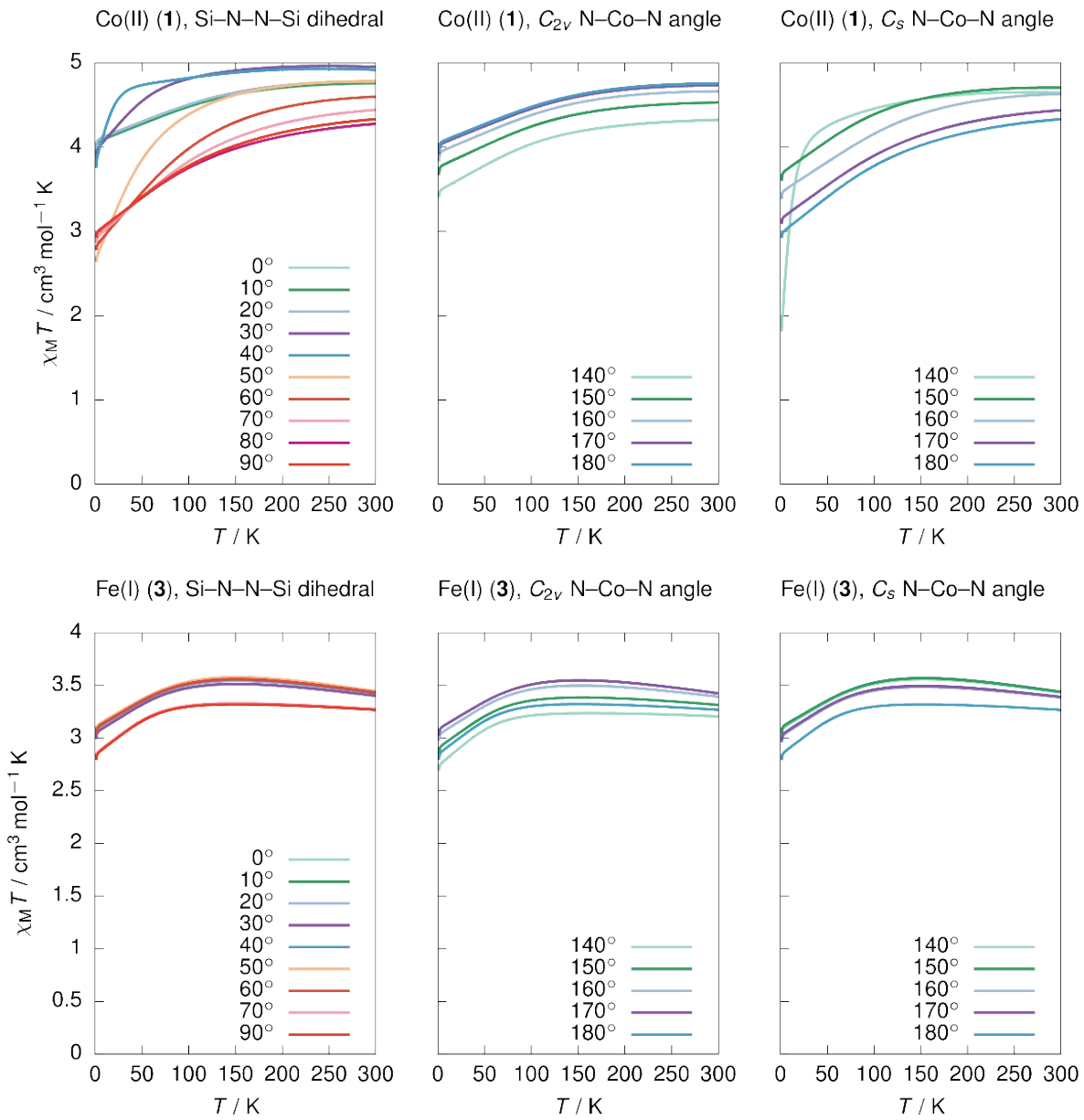


Fig. S2. Temperature-dependent magnetic susceptibilities calculated for the various structures used in the bond angle scans.

Magnetic Measurements

The magnetic susceptibility measurements were obtained using a Quantum Design SQUID magnetometer MPMS-XL7 operating between 1.8 and 300 K. DC measurements were performed on polycrystalline samples of 11 and 12 mg for **1** and **3** respectively. The samples were prepared in a N₂ glovebox (<0.1 ppm H₂O/<0.1 ppm O₂) and static was minimized with a SPI Westek Workstation Ionizer as well as an in-balance ²¹⁰Po static eliminator. The samples were restrained with silicon grease and wrapped in a polyethylene membrane under an inert atmosphere. The samples were subjected to DC fields of -7 to 7 T, and a 3.78 Oe driving field was used for AC measurements. The magnetization data was collected at 100 K to check for ferromagnetic impurities which were absent in all samples. Diamagnetic corrections were applied for the sample holder.

DC Magnetism Plots

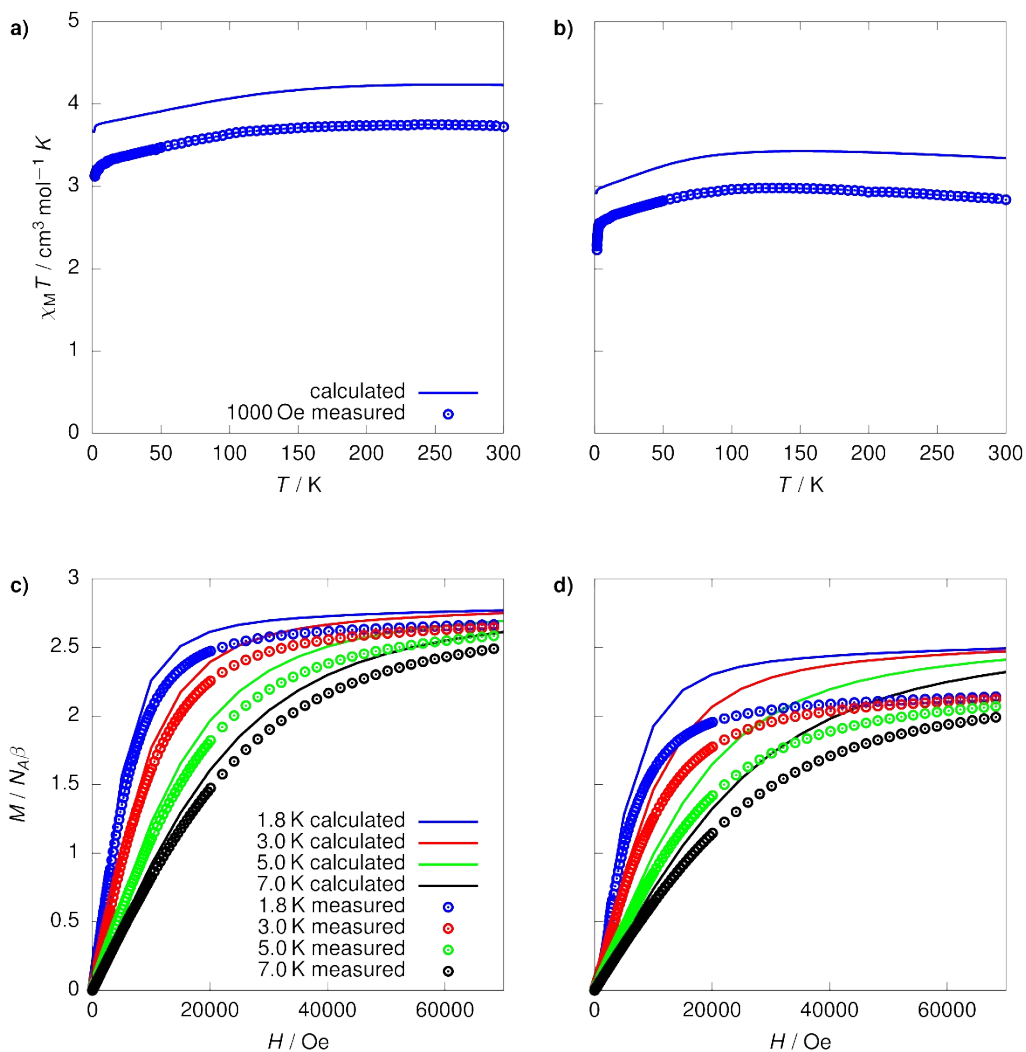


Fig. S3. Comparison of the temperature-dependent magnetic susceptibility calculated for **1** (a) and **3** (b), and isothermal field-dependent magnetization calculated for **1** and **3**, (a and b, respectively). The significant deviation between the calculated and measured magnetization values for **3** most likely results from underestimation of the metal–ligand covalency effect at NEVPT2 level of theory, leading to overestimation of the magnetic anisotropy.²⁴

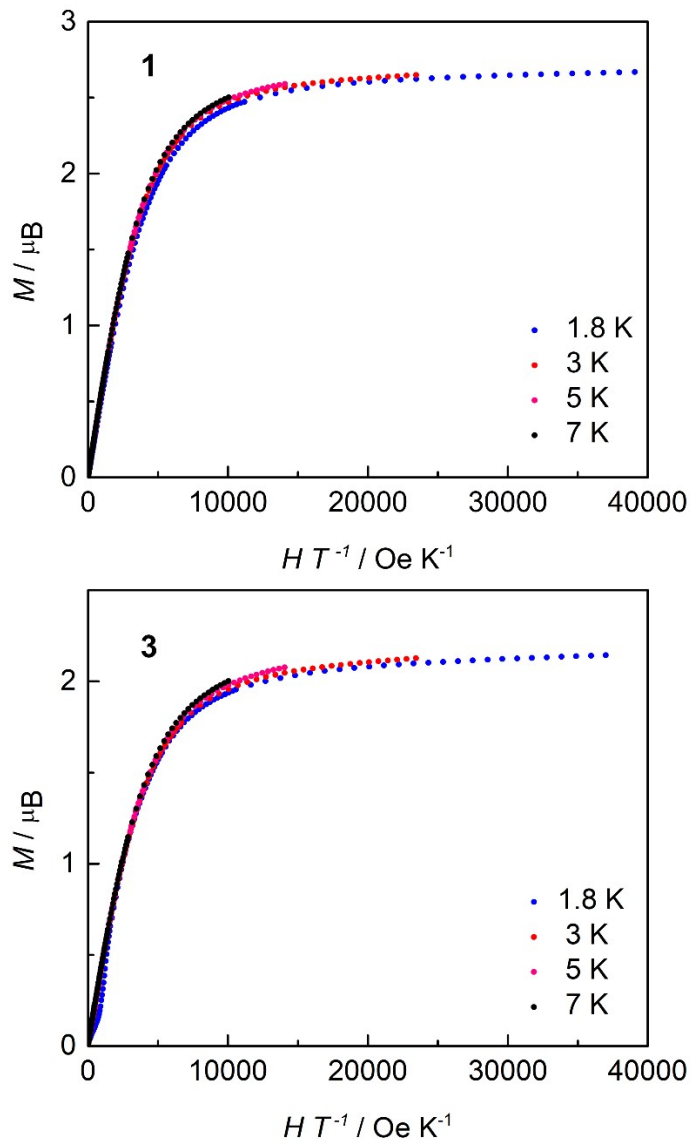


Fig. S4. Solid state field dependence of the reduced magnetization for **1** (top) and **3** (bottom) at the indicated temperatures.

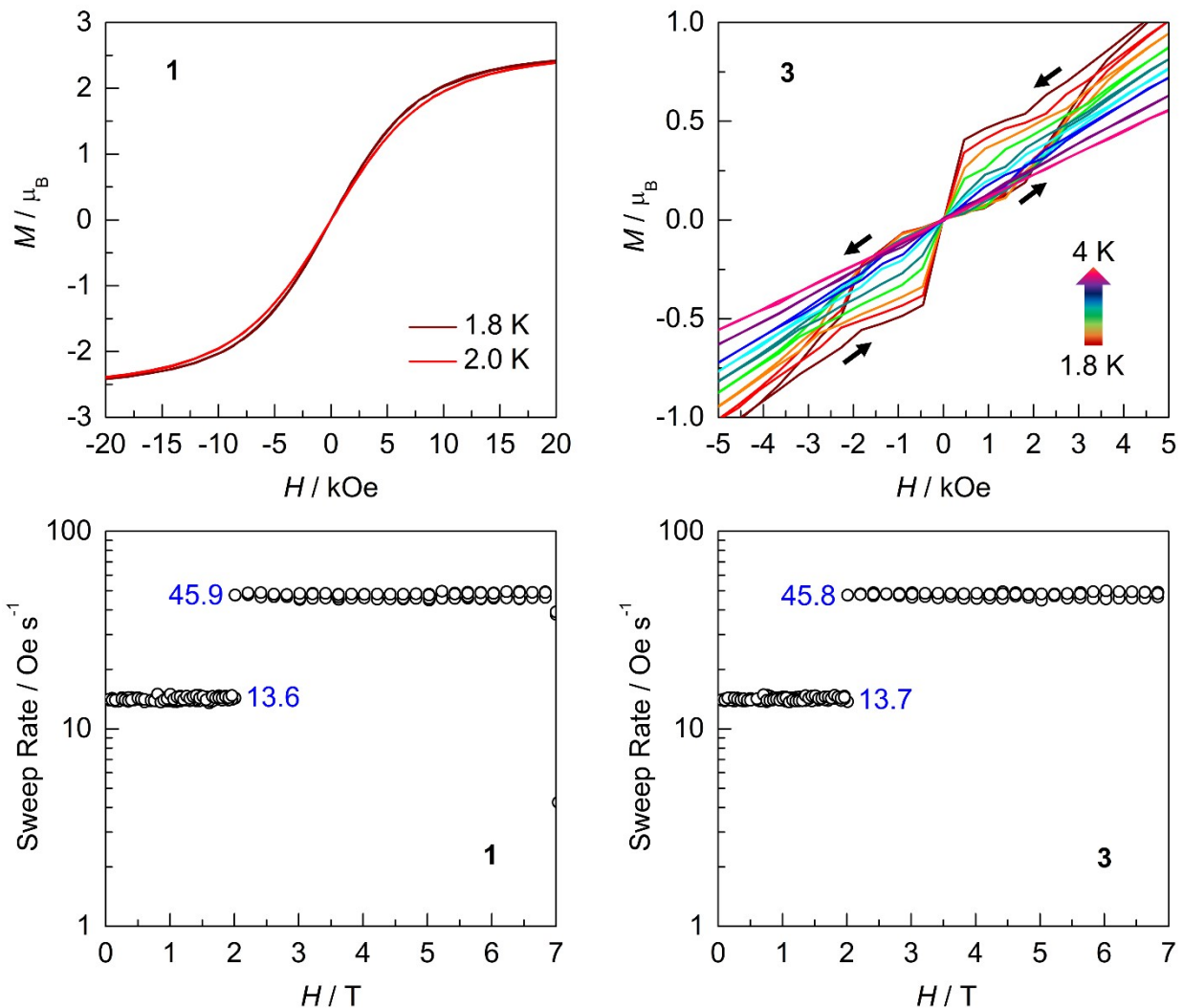


Fig. S5. Magnetic hysteresis data collected on SQUID magnetometer for **1** (left) and **3** (right) at the indicated temperatures (*top*). Black arrows indicated the direction of the field sweep. The average sweep rate was calculated at different field intervals (*bottom*), with a mean field sweep rate of 26.3 Oe s^{-1} (**1**) and 26.4 Oe s^{-1} (**3**) over the entire data range.

AC Magnetism Plots

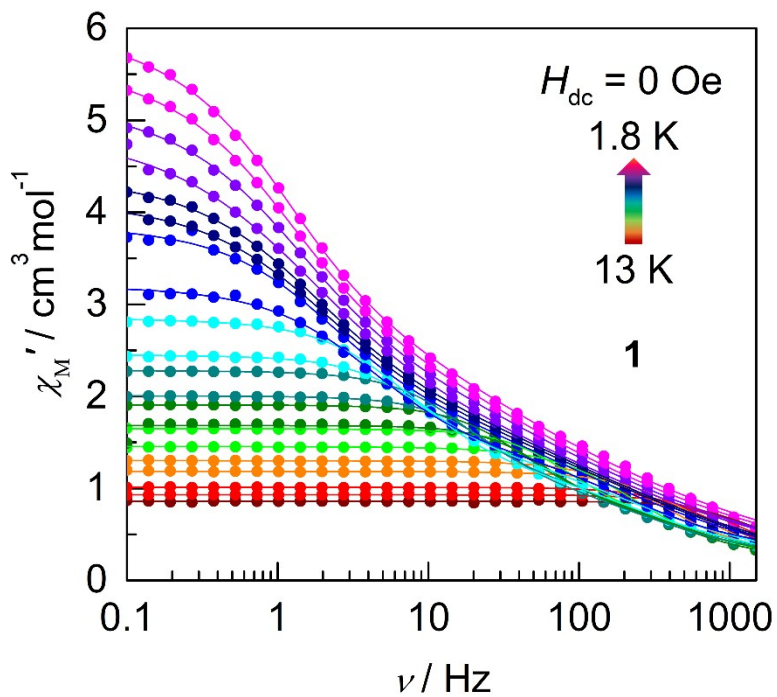


Fig. S6. Frequency dependence of χ_M' as a function of temperature in the range 1.8-13 K in the absence of an applied static field ($H_{dc} = 0$ Oe) for compound **1**. Solid lines represent best fits to the generalized Debye model. Best fit parameters are summarized in Table S6.

Table S6. Best-fit parameters to the generalized Debye model for the frequency dependence of the in-phase magnetic susceptibility (χ_M') as a function of temperature for **1** (Fig. S7). Data collected in the absence of an applied static field ($H_{dc} = 0$ Oe). Values in red were restrained in order to remain physically reasonable. Note: below 8 K, where no reasonable fit could be obtained with a single process generalized Debye model, a double process generalized Debye model was invoked.

T (K)	τ_1 (s)	a_1	χ_{s1}	χ_{T1}	$\chi_T - \chi_s$	τ_2 (s)	a_2	χ_{s2}	χ_{T2}	$\chi_{T2} - \chi_{s2}$
1.8	0.14394	0.18717	0	2.39977	2.39977	0.00562	0.63233	0	3.79366	3.79366
2	0.13823	0.1998	0	2.22099	2.22099	0.00517	0.62656	0	3.56518	3.56518
2.2	0.12227	0.24867	0	2.47123	2.47123	0.00208	0.58538	0	2.77238	2.77238
2.4	0.10114	0.33211	0.0846	2.88002	2.79542	0.00112	0.54368	0	2.00874	2.00874
2.6	0.09296	0.26204	0	2.19401	2.19401	0.00117	0.54174	0	2.22395	2.22395
2.8	0.08033	0.26505	0	2.07717	2.07717	9.73E-04	0.52545	0	2.06723	2.06723
3	0.07383	0.1997	0.05	1.77875	1.72875	0.00132	0.51836	0	2.10226	2.10226
3.5	0.03749	0.21163	0.29708	2.09673	1.79965	7.23E-04	0.27659	0	1.1029	1.1029
4	0.02455	0.10296	0.0316	1.29102	1.25942	7.73E-04	0.41775	0.1036	1.55908	1.45548
4.5	0.01538	0.0551	0.15289	1.20502	1.05213	7.19E-04	0.36332	0.02483	1.24705	1.22221
5	0.00955	0.03314	0.14347	1.10175	0.95828	6.21E-04	0.34528	0.03177	1.1812	1.14943
5.5	0.00615	0.02708	0.14397	1.03403	0.89005	5.48E-04	0.26363	0.08607	0.97217	0.88611
6	0.0041	0.02013	0.06578	0.93392	0.86814	4.02E-04	0.2461	0.12994	0.97446	0.84453
6.5	0.00272	0	0	0.82012	0.82012	3.23E-04	0.12661	0.22933	0.86243	0.6331
7	0.00198	0.00267	0.17437	0.9362	0.76183	2.78E-04	0.21728	0	0.71187	0.71187
8	7.01E-04	0.10775	0.31799	1.45425	1.13626					
9	4.31E-04	0.09195	0.29041	1.30111	1.0107					
10	2.75E-04	0.08436	0.25444	1.18425	0.92981					
11	2.04E-04	0.03831	0.28473	1.01007	0.72534					
12	1.48E-04	0.01271	0.28641	0.9297	0.6433					
13	1.18E-04	6.13E-22	0.3437	0.85851	0.51481					

Table S7. Best-fit parameters to the generalized Debye model for the frequency dependence of the out-of-phase magnetic susceptibility (χ_M'') as a function of temperature for **1** (Fig. 2). Data collected in the absence of an applied static field ($H_{dc} = 0$ Oe). Values in red were restrained in order to remain physically reasonable. Note: below 8 K, where no reasonable fit could be obtained with a single process generalized Debye model, a double process generalized Debye model was invoked.

T (K)	τ_1 (s)	a_1	χ_{s1}	χ_{r1}	$\chi_r - \chi_s$	τ_2 (s)	a_2	χ_{s2}	χ_{r2}	$\chi_{r2} - \chi_{s2}$
1.8	0.12627	0.25646	0.81847	4.08081	3.26234	0.00115	0.59776	0.05846	2.97366	2.91519
2	0.11751	0.26267	1.03287	4.06713	3.03426	0.00105	0.57811	1.2333	3.8667	2.6334
2.2	0.10683	0.23642	1.51385	3.98615	2.4723	0.00133	0.60268	1.13779	3.96221	2.82442
2.4	0.09776	0.24388	0.45261	2.71278	2.26018	0.00117	0.58804	1.46281	4.03719	2.57438
2.6	0.08828	0.23232	0.74679	2.74275	1.99597	0.00123	0.57507	0.94188	3.39296	2.45109
2.8	0.07903	0.19845	2.27743	4.04567	1.76824	0.00125	0.54644	0.42025	2.7458	2.32555
3	0.06817	0.17649	0.15882	1.78175	1.62293	0.00122	0.52315	0.58184	2.73666	2.15482
3.5	0.04276	0.12178	0.0924	1.4076	1.3152	9.58E-04	0.48538	0.70207	2.52545	1.82338
4	0.0254	0.07783	0.17201	1.32799	1.15598	8.10E-04	0.44515	1.35816	2.99788	1.63972
4.5	0.01471	0.06202	0.89834	1.96748	1.06914	5.47E-04	0.40375	0.08291	1.41709	1.33418
5	0.00921	0.04247	0.10412	1.11455	1.01043	4.62E-04	0.35877	0.73719	1.91961	1.18242
5.5	0.00603	0.02399	0.90046	1.80222	0.90176	4.09E-04	0.30587	0.11416	1.10945	0.9953
6	0.00392	0.02657	0.91306	1.7953	0.88224	3.20E-04	0.2974	0.28745	1.21255	0.92511
6.5	0.00266	0.0197	0.23507	1.07247	0.8374	2.47E-04	0.24487	0.74793	1.51397	0.76604
7	0.00185	0.03211	0.67847	1.52839	0.84992	2.14E-04	0.21258	0.35582	1.04704	0.69122
8	8.26E-04	0.0787	0.20118	1.20171	1.00053	9.75E-05	1.0E-03	0.49216	0.7946	0.3024
9	4.06E-04	0.10065	0.00256	1.08205	1.07949					
10	2.62E-04	0.0765	0.01784	0.99502	0.97718					
11	1.56E-04	0.09388	0.02402	0.90305	0.87904					
12	9.78E-04	0.11927	0.16746	1.06218	0.89472					
13	9.51E-05	0.03049	0.0047	0.68281	0.67811					

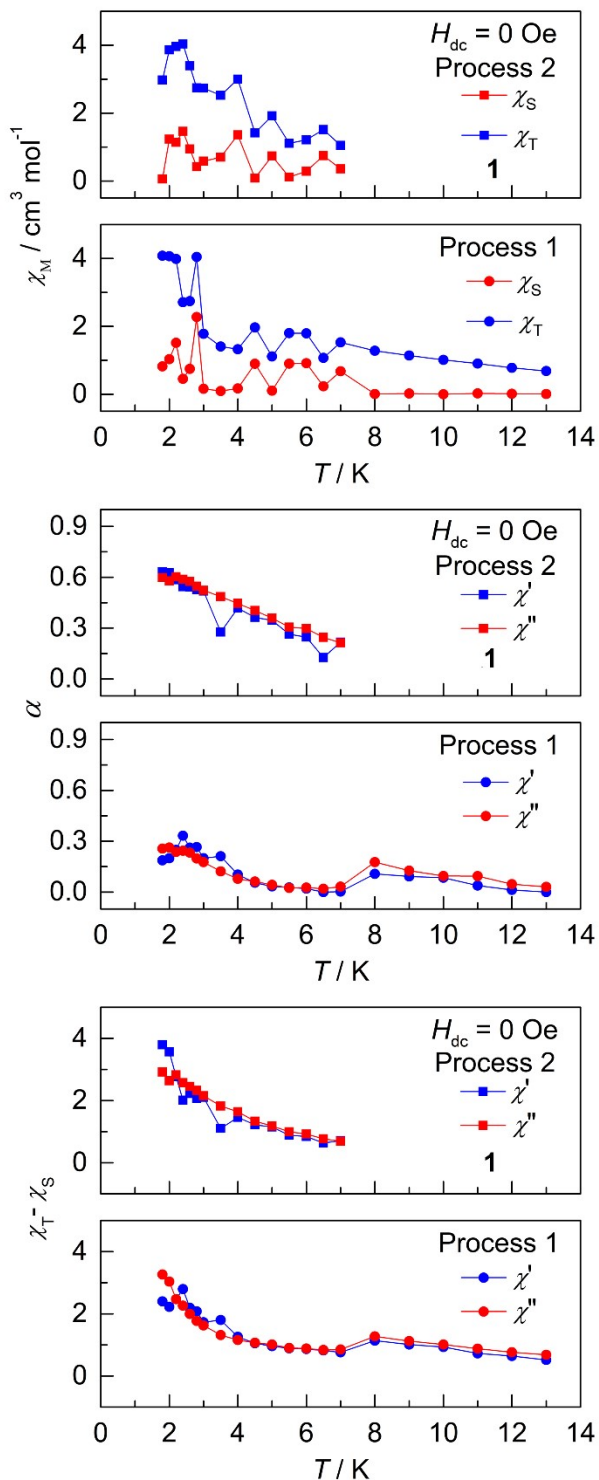


Fig. S7. Data obtained from the generalized Debye fits of χ_M' and χ_M'' frequency dependent ac data collected in the absence of an applied static field ($H_{dc} = 0$ Oe) for compound **1**. Temperature dependence of χ_T and χ_S (*top*), α (*middle*), and $\chi_T - \chi_S$ (*bottom*).

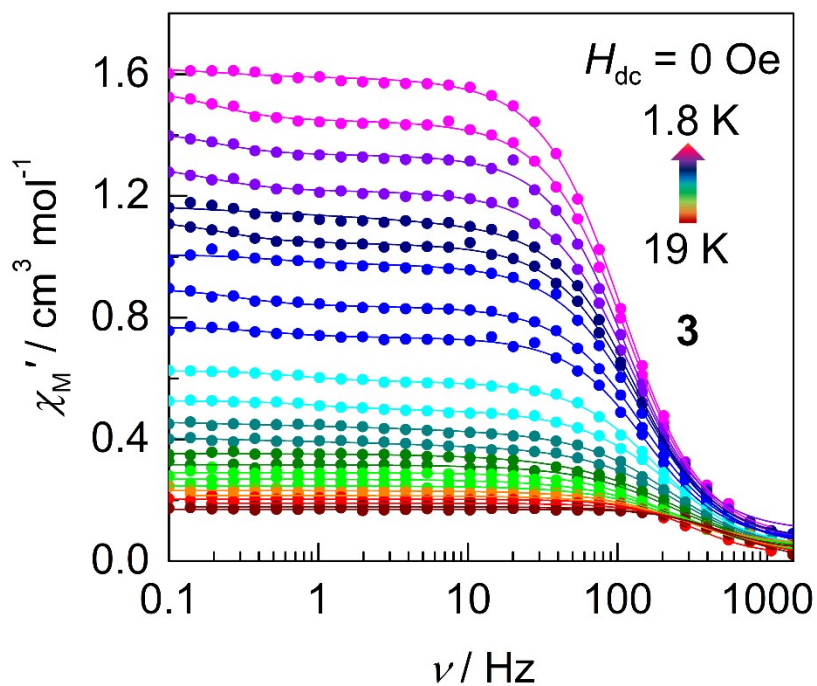


Fig. S8. Frequency dependence of χ_M' as a function of temperature in the range 1.8-19 K in the absence of an applied static field ($H_{dc} = 0$ Oe) for compound **3**. Solid lines represent best fits to the generalized Debye model. Best fit parameters are summarized in Table S8.

Table S8. Best-fit parameters to the generalized Debye model for the frequency dependence of the in-phase magnetic susceptibility (χ_M') as a function of temperature for **3** (Fig. S9). Data collected in the absence of an applied static field ($H_{dc} = 0$ Oe). Values in red were restrained in order to remain physically reasonable. Note: below 9 K, where no reasonable fit could be obtained with a single process generalized Debye model, a double process generalized Debye model was invoked.

T (K)	τ_1 (s)	a_1	χ_{s1}	χ_{t1}	$\chi_t - \chi_s$	τ_2 (s)	a_2	χ_{s2}	χ_{t2}	$\chi_{t2} - \chi_{s2}$
1.8	0.00149	0.09135	4.24356 E-4	1.52569	1.52527	0.79738	0.10746	0.06505	0.09723	0.03218
2	0.0014	0.07886	0.057	1.44768	1.39068	0.81756	0	0.00134	0.10269	0.10135
2.2	0.00143	0.09724	0.04504	1.2862	1.24116	0.81275	0	0.05021	0.12821	0.078
2.4	0.0013	0.10813	5.14724 E-4	1.16115	1.16064	0.84214	0.02863	0.0565	0.13796	0.08146
2.6	0.00125	0.09837	0.02351	1.03573	1.01222	0.53784	0.81108	0.00856	0.22113	0.21257
2.8	0.00118	0.07403	8.39735 E-4	0.99932	0.99848	0.69244	0	0.04684	0.11841	0.07157
3	0.00114	0.11298	0.00969	0.94684	0.93715	0.32248	0	0.03189	0.05983	0.02794
3.5	0.00108	0.16797	0.00489	0.79108	0.78619	0.56031	0	0.04805	0.10407	0.05602
4	0.00105	0.13564	0.00988	0.6818	0.67192	0.32787	0	0.05477	0.08651	0.03174
5	8.71521 E-4	0.12978	0.0129	0.56883	0.55593	0.22353	0	0.02359	0.05672	0.03313
6	6.73288 E-4	0.22568	0	0.50147	0.50147	0.17388	0	0	0.02523	0.02523
7	7.13619 E-4	0.16478	0	0.37746	0.37746	0.06787	0	0	0.12394	0.12394
8	6.46612 E-4	0.11798	0	0.32915	0.32915	0.03143	0.81403	0	0.1103	0.1103
9	6.21851 E-4	0.19472	0	0.35306	0.35306					
10	6.66211 E-4	0.15075	0.02817	0.31679	0.28862					
11	7.77227 E-4	0.13779	0.04474	0.29061	0.24587					
12	5.45657 E-4	0.12672	0.00981	0.26955	0.25974					
13	5.41749 E-4	0.02855	0.01434	0.24724	0.23289					
14	5.5143E -4	0.07406	0.02648	0.23136	0.20488					
15	5.26648 E-4	0.07051	0.04617	0.21488	0.16871					
16	5.01879 E-4	0	0.01703	0.20283	0.1858					
17	3.60566 E-4	0.09135	0.01505	0.19019	0.17514					
18	2.94644 E-4	0.07886	0	0.17838	0.17838					
19	3.37912 E-4	0.09724	0.03659	0.16999	0.1334					

Table S9. Best-fit parameters to the generalized Debye model for the frequency dependence of the out-of-phase magnetic susceptibility (χ_M'') as a function of temperature for **3** (Fig. 2). Data collected in the absence of an applied static field ($H_{dc} = 0$ Oe). Values in red were restrained in order to remain physically reasonable. Note: below 9 K, where no reasonable fit could be obtained with a single process generalized Debye model, a double process generalized Debye model was invoked.

T (K)	τ_1 (s)	a_1	χ_{s1}	χ_{r1}	$\chi_{r1} - \chi_s$	τ_2 (s)	a_2	χ_{s2}	χ_{r2}	$\chi_{r2} - \chi_{s2}$
1.8	0.00144	0.09893	0.0029	0.81994	0.81704	0.92056	0	0.76787	0.86273	0.09485
2	0.00133	0.09241	0.01724	0.80559	0.78835	0.83611	0	0.77161	0.85899	0.08739
2.2	0.00129	0.09498	0.0428	0.78003	0.73722	0.834	0.02531	0.77221	0.85839	0.08618
2.4	0.00124	0.10549	0.0603	0.76252	0.70222	0.86379	0.09314	0.77785	0.85274	0.07489
2.6	0.00125	0.09681	0.08513	0.73769	0.65087	0.720	0.01187	0.78357	0.84767	0.00624
2.8	0.00121	0.09131	0.11296	0.74778	0.63482	0.69191	0.08388	0.779	0.84556	0.06657
3	0.00115	0.08732	0.12971	0.73103	0.60132	0.600	0.03535	0.7853	0.83926	0.05203
3.5	0.00108	0.10925	0.13869	0.68414	0.54546	0.53024	0.04452	0.78725	0.84335	0.0561
4	0.00101	0.10831	0.15751	0.66532	0.50781	0.40475	0	0.79225	0.83835	0.0461
5	9.09264 E-4	0.11251	0.1901	0.63273	0.44263	0.26604	0.0655	0.79615	0.83445	0.0383
6	7.88153 E-4	0.15174	0.20167	0.62116	0.4195	0.14831	0	0.80229	0.82831	0.02601
7	7.25925 E-4	0.15214	0.22679	0.59604	0.36926	0.06667	0	0.80486	0.82574	0.02088
8	6.85726 E-4	0.14652	0.24427	0.57856	0.33429	0.0312	0	0.80572	0.82553	0.01981
9	6.3159E -4	0.19826	0.21066	0.53628	0.32562					
10	6.25917 E-4	0.18667	0.21638	0.51685	0.30047					
11	5.97411 E-4	0.17013	0.23025	0.50701	0.27676					
12	6.50725 E-4	0.10126	0.28963	0.52312	0.23349					
13	5.26941 E-4	0.16924	0.26477	0.50368	0.23891					
14	5.00978 E-4	0.14153	0.30419	0.51556	0.21137					
15	4.5965E -4	0.24756	0.3257	0.5378	0.2121					
16	4.16919 E-4	0.06433	0.33298	0.51654	0.18356					
17	3.58611 E-4	0.11187	0.31229	0.5	0.18771					
18	3.52484 E-4	0.05169	0.35617	0.51392	0.15775					
19	2.86941 E-4	0.06869	0.33651	0.50027	0.16376					

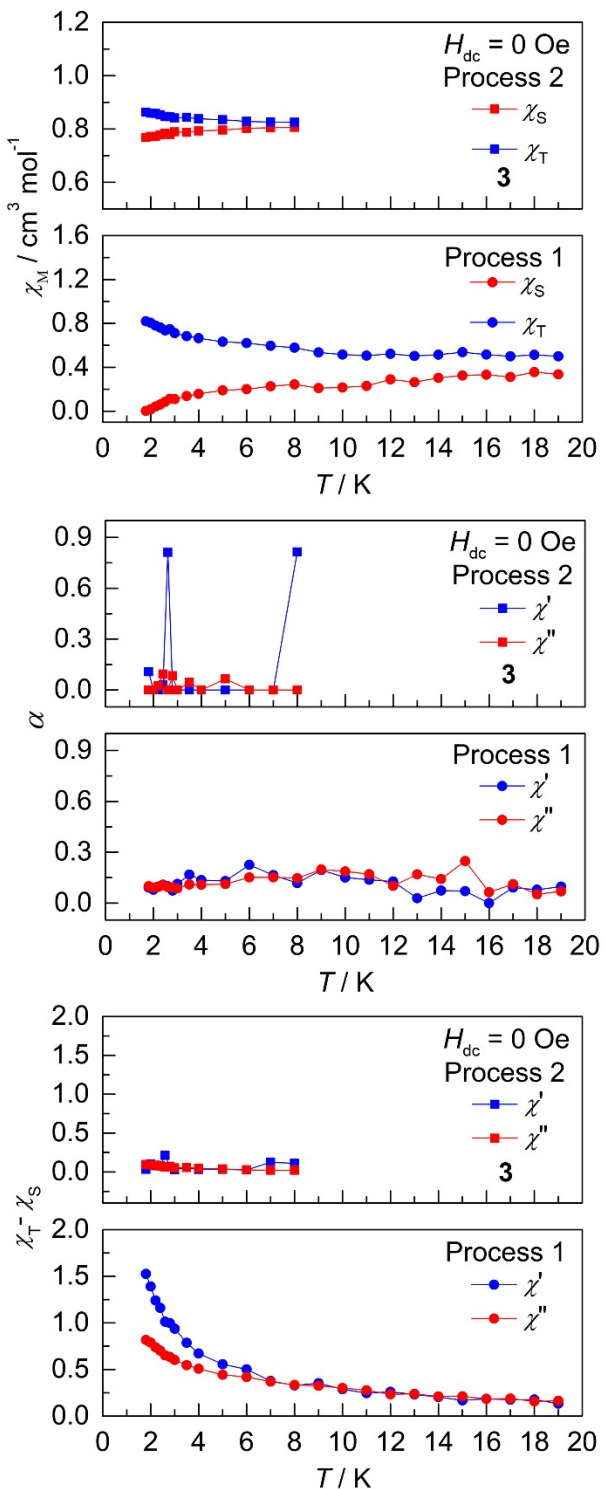


Fig. S9. Data obtained from the generalized Debye fits of χ_M' and χ_M'' frequency dependent ac data collected in the absence of an applied static field ($H_{dc} = 0$ Oe) for compound **3**. Temperature dependence of χ_T and χ_S (*top*), α (*middle*), and $\chi_T - \chi_S$ (*bottom*).

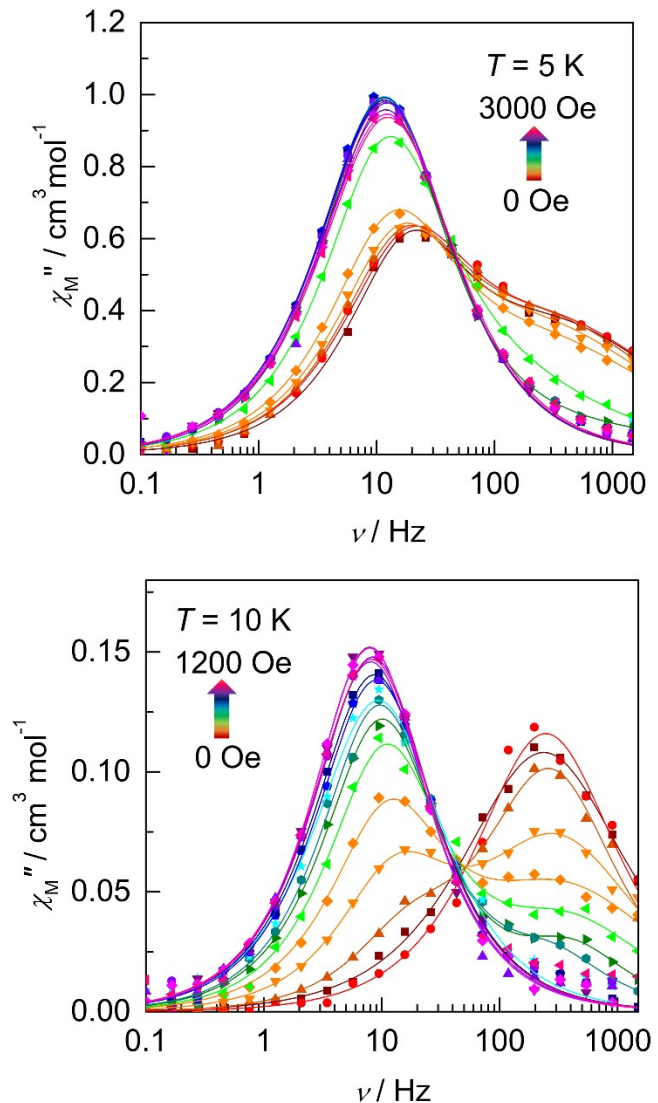


Fig. S10. Frequency dependence of χ_M'' as a function of field in the range 0-1200 Oe, for compound **3** (*top*) and 0-3000 Oe for compound **1** (*bottom*). Data were collected at constant temperature of 10 K and 5 K for compounds **3** and **1**, respectively. Solid lines represent best fits to the generalized Debye model. Best fit parameters are summarized in Table S10 (**1**) and Table S11 (**3**).

Table S10. Best-fit parameters to the generalized Debye model for the frequency dependence of the out-of-phase magnetic susceptibility (χ_M'') as a function of field for **1** collected at $T = 5$ K (Fig. S11; *top*). Note: below 1400 Oe, where no reasonable fit could be obtained with a single process generalized Debye model, a double process generalized Debye model was invoked.

H (Oe)	τ_1 (s)	α_1	χ_{s1}	χ_{r1}	$\chi_{r1} - \chi_{s1}$	τ_2 (s)	α_2	χ_{s2}	χ_{r2}	$\chi_{r2} - \chi_{s2}$
0	0.00856	0.03025	0.07108	1.10759	1.03652	4.00305 E-4	0.37273	0.03763	1.24045	1.20282
200	0.00864	0.07851	1E-5	1.15339	1.15338	3.8577E -4	0.37393	0.22932	1.41516	1.18584
400	0.00943	0.06062	0.18817	1.29943	1.11126	4.60708 E-4	0.36843	0.22381	1.42435	1.20054
600	0.01022	0.062	0.26299	1.40087	1.13788	4.89385 E-4	0.37892	0.93355	2.09238	1.15883
800	0.01136	0.06154	0.27603	1.53271	1.25668	4.88249 E-4	0.39151	1.92638	2.9832	1.05682
1000	0.0128	0.04655	0.20707	1.91086	1.70379	0.00129	0.39682	0.18205	0.78971	0.60765
1200	0.0139	0.05631	0.0217	2.13396	2.11226	2.59562 E-4	0.45795	2.4228	2.6772	0.2544
1400	0.01364	0.08645	0.05385	2.32511	2.27126					
1600	0.01366	0.08682	0.01314	2.2945	2.28136					
1800	0.01366	0.08807	5.49393 E-4	2.28129	2.28074					
2000	0.01358	0.08936	8.22336 E-4	2.26849	2.26767					
2200	0.01347	0.09158	0.00573	2.26972	2.26399					
2400	0.01294	0.07602	0.00489	2.20824	2.20335					
2600	0.0133	0.09286	0.00282	2.22132	2.21851					
2800	0.01294	0.1042	0.00124	2.23098	2.22973					
3000	0.01274	0.10176	0.0038	2.20496	2.20116					

Table S11. Best-fit parameters to the generalized Debye model for the frequency dependence of the out-of-phase magnetic susceptibility (χ_M'') as a function of field for **3** collected at $T = 10$ K (Fig. S11; *bottom*). Note: in the range 40-140 Oe, no reasonable fit could be obtained with a single process generalized Debye model, a double process generalized Debye model was invoked.

H (Oe)	τ_1 (s)	a_1	χ_{s1}	χ_{t1}	$\chi_{t1} - \chi_{s1}$	τ_2 (s)	a_2	χ_{s2}	χ_{t2}	$\chi_{t2} - \chi_{s2}$
0						6.7391E -4	0.20014	0.23267	0.5304	0.29773
20						6.46792 E-4	0.11955	0.24094	0.52122	0.28027
40	0.00921	0	0.95487	1.01017	0.0553	5.87446 E-4	0.08493	1.30217	1.52598	0.22381
60	0.01205	0	0.39814	0.50211	0.10398	5.03527 E-4	0.19999	0.85571	1.04751	0.1918
80	0.01393	0	0.36886	0.52294	0.15408	4.3463E -4	0.29088	0.86269	1.02145	0.15876
100	0.01471	0	0.30264	0.51558	0.21294	4.0181E -4	0.20172	0.57358	0.67202	0.09844
120	0.01591	0.00816	0.26578	0.51082	0.24505	3.85136 E-4	0	0.62265	0.67126	0.04861
140	0.01668	0.0057	0.28666	0.54214	0.25548	5.71829 E-4	0	0.48588	0.52585	0.03997
160	0.01697	0.06485	0.32716	0.61469	0.28753					
180	0.01772	0.02801	0.31505	0.60409	0.28904					
200	0.01831	0.03112	0.28859	0.58381	0.29522					
400	0.01903	0.01893	0.31272	0.61757	0.30485					
600	0.01972	0.0169	0.31717	0.61695	0.29979					
800	0.0201	0	0.28669	0.59087	0.30417					
1000	0.02006	0.00189	1.01606	1.32043	0.30437					
1200	0.01936	0.02596	0.29103	0.59737	0.30634					

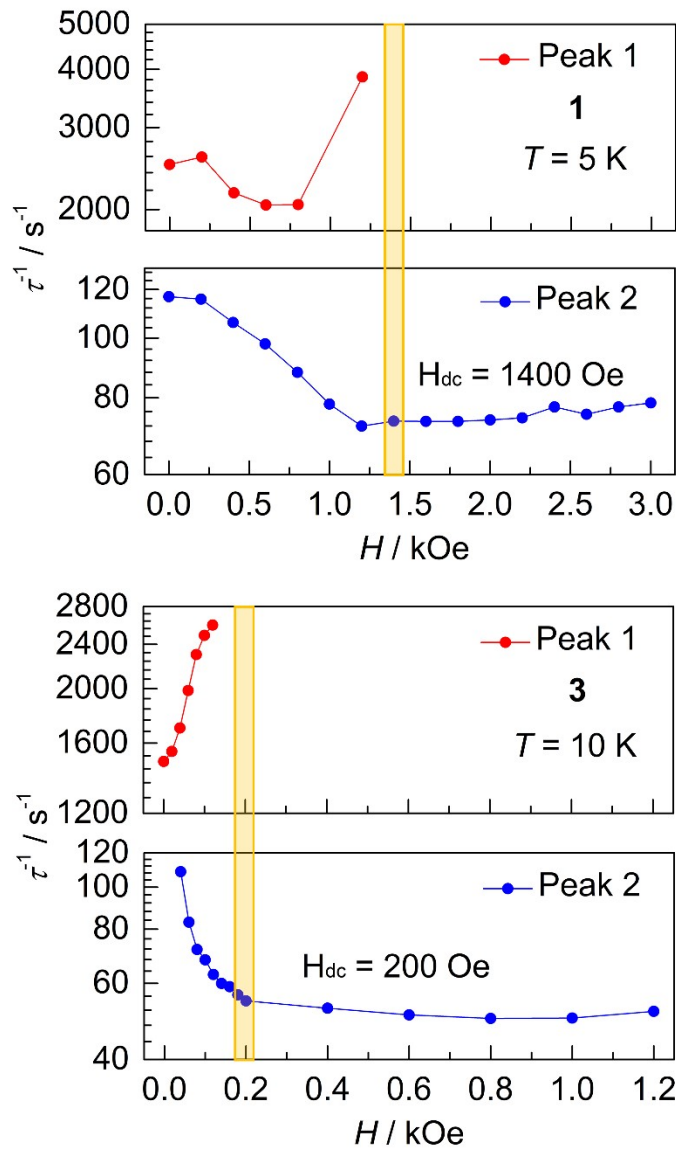


Fig. S11. Field dependence of the relaxation times (τ) at a fixed temperature of 5 K for compound 1 (top) and 10 K for compound 3 (bottom). The relaxation times were obtained from the generalized Debye model (see, Tables S10 and S11). The minimum represents the optimal static field for which the relaxation time is longest and quantum tunneling of the magnetization is reduced, and the high frequency peak (red) is eradicated. This is the field at which temperature dependent relaxation studies were completed at (*vide infra*).

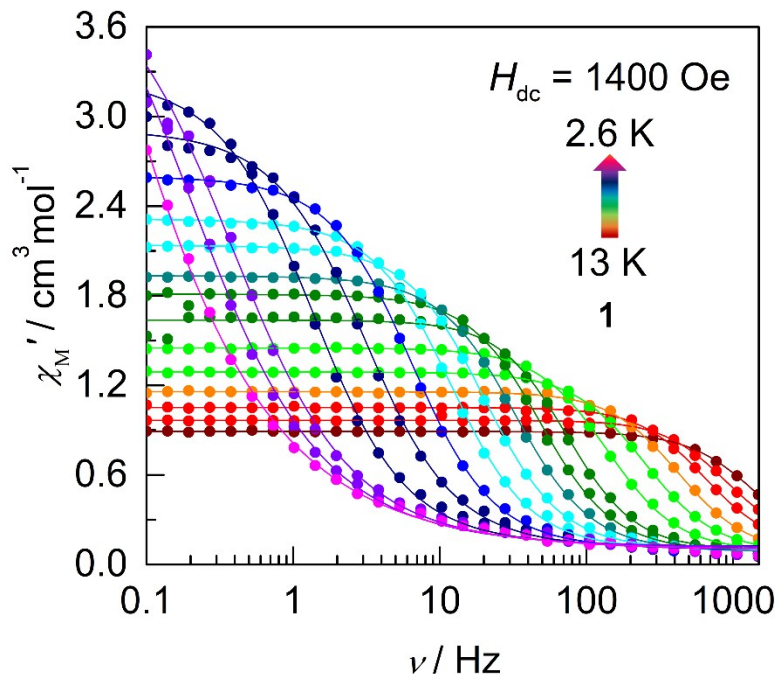


Fig. S12. Frequency dependence of χ_M' as a function of temperature in the range 2.6-13 K in the presence of an applied static field ($H_{\text{dc}} = 1400$ Oe) for compound **1**. Solid lines represent best fits to the generalized Debye model. Best fit parameters are summarized in Table S12.

Table S12. Best-fit parameters to the generalized Debye model for the frequency dependence of the in-phase magnetic susceptibility (χ_M') as a function of temperature for **1** (Fig. S13). Data collected in the presence of an applied static field ($H_{dc} = 1400$ Oe).

T (K)	τ (s)	α	χ_s	χ_T	$\chi_T - \chi_s$
2.6	4.1955	0.39938	0.09737	8.42495	8.32762
2.8	0.81819	0.30691	0.11673	4.83546	4.71872
3	0.42163	0.26622	0.11559	4.16716	4.05157
3.5	0.11798	0.16038	0.12112	3.27503	3.15391
4	0.05184	0.14368	0.10518	2.91913	2.81395
4.5	0.02482	0.10529	0.10096	2.60346	2.5025
5	0.01338	0.08675	0.09737	2.31513	2.21776
5.5	0.00795	0.07529	0.09613	2.13825	2.04212
6	0.0049	0.07311	0.08345	1.93416	1.85072
6.5	0.00328	0.05397	0.08978	1.81004	1.72026
7	0.00217	0.03169	0.09643	1.63716	1.54073
8	0.00115	0.04557	0.08641	1.45052	1.36411
9	6.41E-04	0.04976	0.07782	1.2898	1.21198
10	3.78E-04	0.03627	0.07482	1.15738	1.08257
11	2.49E-04	0.01879	0.11361	1.05157	0.93795
12	1.78E-04	0	0.15266	0.96507	0.81241
13	1.07E-04	0.04075	0.04448	0.89138	0.8469

Table S13. Best-fit parameters to the generalized Debye model for the frequency dependence of the out-of-phase magnetic susceptibility (χ_M'') as a function of temperature for **1** (Fig. 2). Data collected in the presence of an applied static field ($H_{dc} = 1400$ Oe).

T (K)	τ (s)	α	χ_s	χ_T	$\chi_T - \chi_s$
2.6	1.14792	0.32111	3.00379	7.35993	4.35614
2.8	0.55909	0.23924	1.48248	5.23773	3.75525
3	0.29545	0.14659	1.87261	5.10558	3.23297
3.5	0.11778	0.13803	0.55443	3.62018	3.06575
4	0.05009	0.09802	0.50002	3.17341	2.67339
4.5	0.02496	0.09676	0.36843	2.84722	2.47879
5	0.01355	0.08751	0.44319	2.65689	2.2137
5.5	0.00792	0.07854	0.10115	2.16041	2.05927
6	0.00489	0.0789	0.48686	2.36041	1.87356
6.5	0.00325	0.07028	0.10124	1.85534	1.7541
7	0.00222	0.0632	0.10175	1.68968	1.58794
8	0.00112	0.05607	0.10034	1.49616	1.39582
9	6.21E-04	0.04937	0.01551	1.2515	1.23599
10	3.68E-04	0.03397	0.02611	1.12235	1.09624
11	2.38E-04	0.02466	0.07309	1.05518	0.98208
12	1.57E-04	0.03802	0.08842	1.01006	0.92163
13	1.08E-04	0.02761	0.07263	0.8913	0.81867

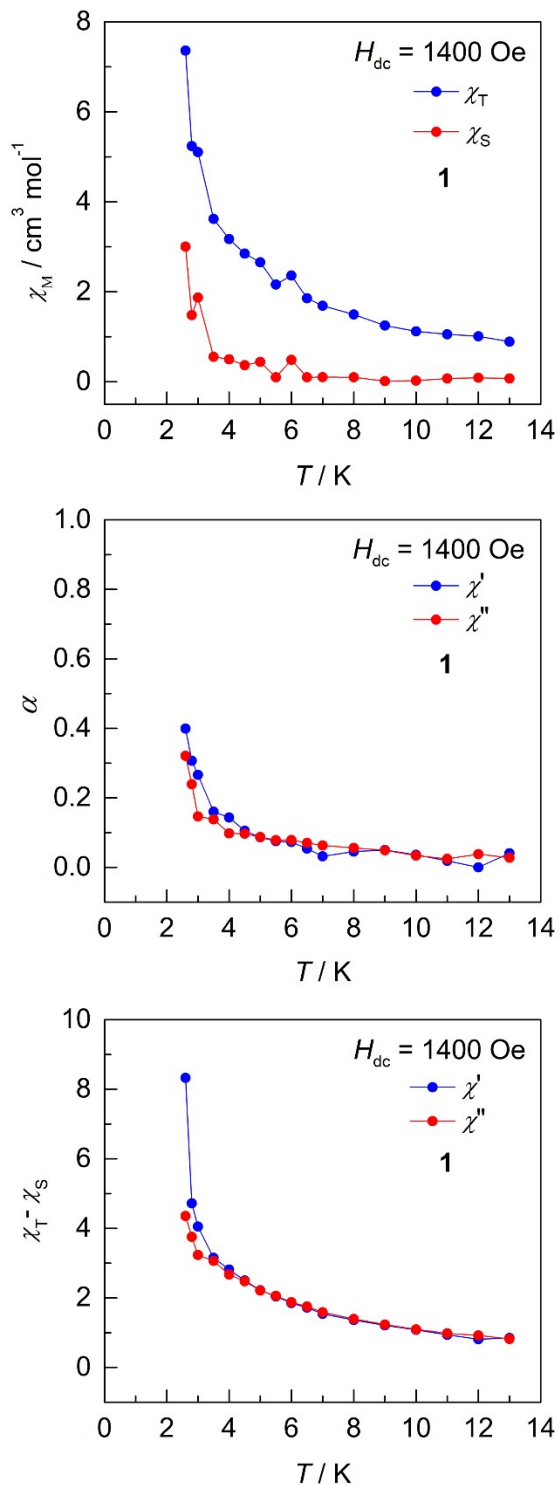


Fig. S13. Data obtained from the generalized Debye fits of χ_M' and χ_M'' frequency dependent ac data collected under an applied static field ($H_{dc} = 1400$ Oe) for compound **1**. Temperature dependence of χ_T and χ_S (*top*), α (*middle*), and $\chi_T - \chi_S$ (*bottom*).

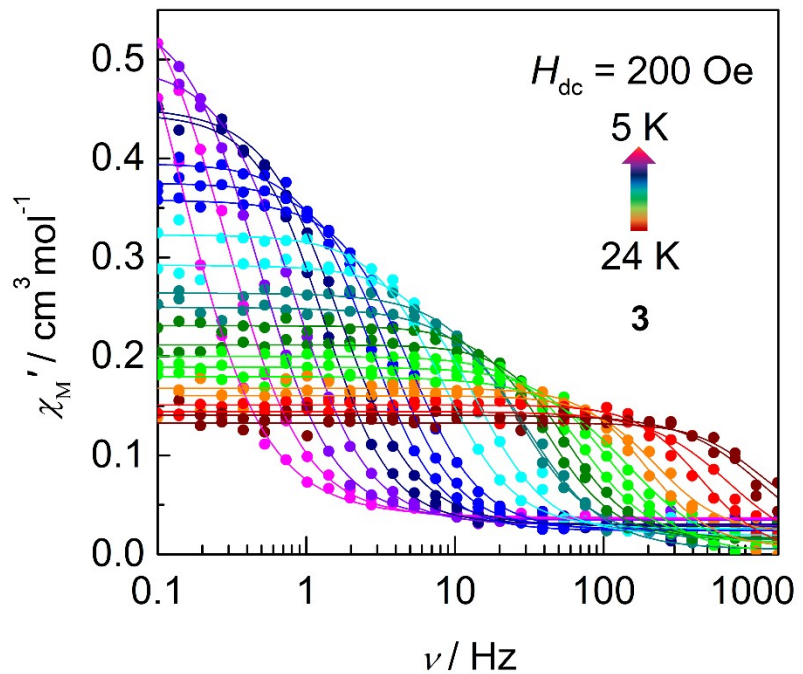


Fig. S14. Frequency dependence of χ_M' as a function of temperature in the range 5-24 K in the presence of an applied static field ($H_{dc} = 200$ Oe) for compound **3**. Solid lines represent best fits to the generalized Debye model. Best fit parameters are summarized in Table S14.

Table S14. Best-fit parameters to the generalized Debye model for the frequency dependence of the in-phase magnetic susceptibility (χ_M') as a function of temperature for **3** (Fig. S15). Data collected in the presence of an applied static field ($H_{dc} = 200$ Oe).

T (K)	τ (s)	α	χ_s	χ_T	$\chi_T - \chi_s$
5	1.15146	0.11346	0.03685	0.73199	0.69515
5.5	0.55605	0.07725	0.03563	0.60504	0.56941
6	0.33356	0.05828	0.03434	0.55045	0.51612
6.5	0.19217	0.05314	0.02941	0.49375	0.46434
7	0.12183	0.02088	0.0305	0.445	0.4145
7.5	0.09511	0.0693	0.02803	0.45231	0.42428
8	0.05831	0.02163	0.02395	0.39486	0.37091
8.5	0.04385	0.02209	0.02587	0.37517	0.34931
9	0.03207	0.03956	0.02392	0.35812	0.3342
10	0.01931	0.04578	0.02547	0.32306	0.29759
11	0.01139	0.04577	0.01918	0.29215	0.27298
12	0.0061	0.06331	0.01422	0.26414	0.24992
13	0.00521	0.07833	0.00451	0.24969	0.24518
14	0.00387	0.01985	0.01582	0.23102	0.2152
15	0.0028	0	0.01646	0.2116	0.19514
16	0.00215	0.03409	0.01153	0.20003	0.1885
17	0.00145	0.05332	1E-3	0.18921	0.18821
18	0.00109	0.10809	1E-4	0.17962	0.17952
19	8.12207E-4	0.00358	0.00706	0.16772	0.16066
20	7.10087E-4	0.01571	0.02102	0.16032	0.1393
21	3.54307E-4	0	0.00229	0.15085	0.14856
22	2.27955E-4	0.08182	1E-4	0.14439	0.14429
23	1.35706E-4	0.09303	1E-4	0.1408	0.1407
24	1.44368E-4	0	0.03021	0.13263	0.10242

Table S15. Best-fit parameters to the generalized Debye model for the frequency dependence of the out-of-phase magnetic susceptibility (χ_M'') as a function of temperature for **3** (Fig. 2). Data collected in the presence of an applied static field ($H_{dc} = 200$ Oe).

T (K)	τ (s)	α	χ_s	χ_T	$\chi_T - \chi_s$
5	1.0449	0.0782	7.23615	7.85955	0.62341
5.5	0.52831	0.05029	3.33683	3.87171	0.53488
6	0.30685	0.05359	1.24111	1.7361	0.495
6.5	0.19642	0.04754	0.66127	1.12081	0.45954
7	0.12299	0.01141	0.57171	0.98948	0.41777
7.5	0.08591	0.03344	0.39665	0.7954	0.39874
8	0.05896	0.02834	0.37468	0.74781	0.37313
8.5	0.04362	0.02586	0.26142	0.61277	0.35135
9	0.03199	0.01672	0.25824	0.58453	0.3263
10	0.01877	0.02002	0.2315	0.52998	0.29848
11	0.01125	0.0229	0.33862	0.61392	0.2753
12	0.00746	0.03809	0.29144	0.5446	0.25317
13	0.0054	0.01614	0.31703	0.53868	0.22165
14	0.00383	0.03741	0.31593	0.53211	0.21618
15	0.00285	0.04712	0.3134	0.51436	0.20097
16	0.00207	0.01651	0.33638	0.51969	0.18331
17	0.0016	0.00988	0.32039	0.50021	0.17982
18	0.00116	0.04057	0.3305	0.50015	0.16965
19	8.35463E-4	0.05857	0.35924	0.51353	0.15428
20	5.79612E-4	0.11466	0.34287	0.51354	0.17067
21	3.69846E-4	0.10542	0.35228	0.50773	0.15545
22	2.36987E-4	0.05545	0.3549	0.50323	0.14833
23	1.24452E-4	0.10147	0.00566	0.17972	0.17406
24	8.67841E-5	0.17117	5.67676E-4	0.17266	0.17209

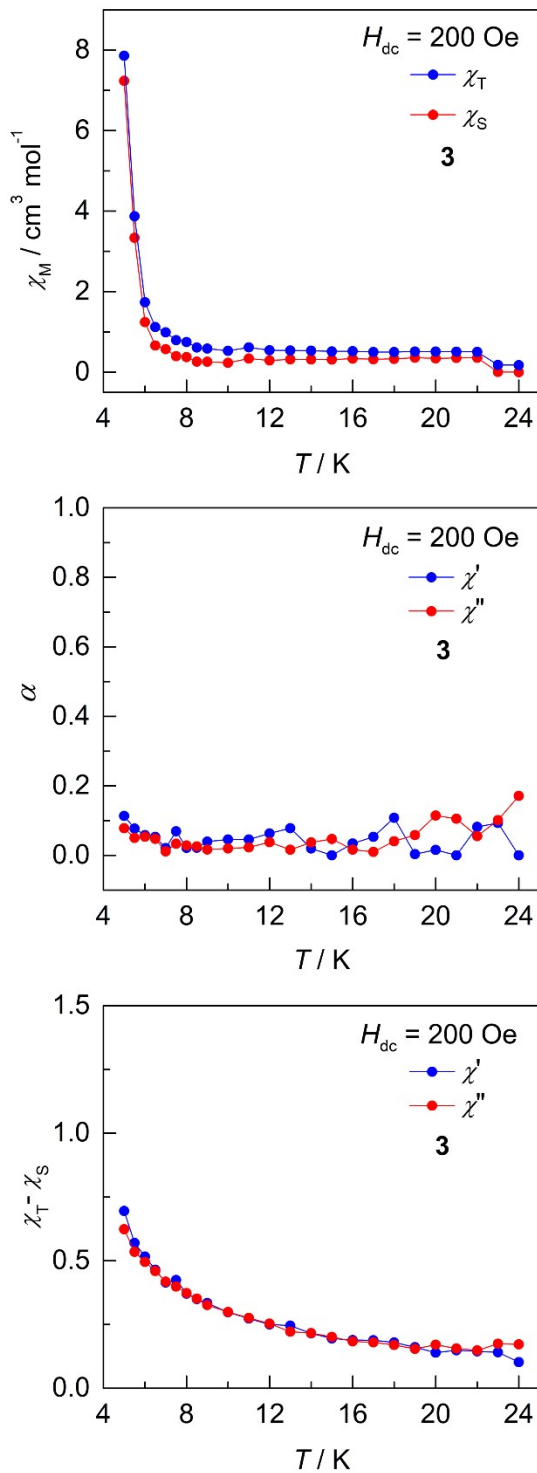


Fig. S15. Data obtained from the generalized Debye fits of χ_M' and χ_M'' frequency dependent ac data collected under an applied static field ($H_{dc} = 200$ Oe) for compound **3**. Temperature dependence of χ_T and χ_S (*top*), α (*middle*), and $\chi_T - \chi_S$ (*bottom*).

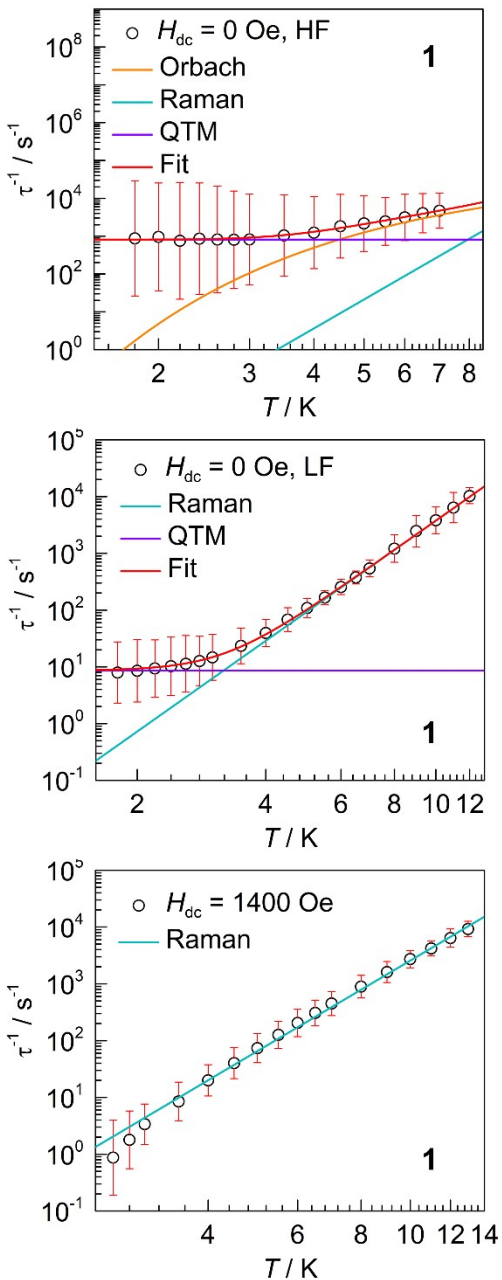


Fig. S16. Temperature dependence of the relaxation times (τ) for compound **1** collected under zero applied static field ($H_{dc} = 0 \text{ Oe}$; *top* and *middle*) and under an applied static field ($H_{dc} = 1400 \text{ Oe}$; *bottom*). The red solid lines represent the best fit to Eqn. S2. The orange, teal, and purple lines are the individual components of the magnetization relaxation for Orbach, Raman, and QTM processes, respectively. A single relaxation mechanism was used to describe the dynamics when only one component is presented. Parameters are summarized in Table S16. The error bars on the

relaxation time have been calculated from the α -parameters of the generalized Debye fit with the log-normal distribution.¹⁸

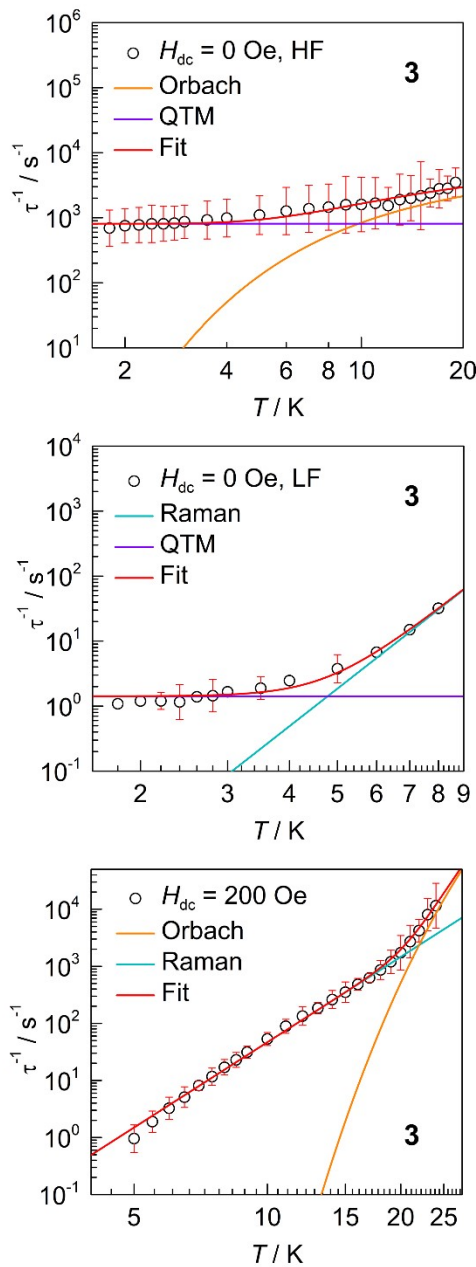


Fig. S17. Temperature dependence of the relaxation times (τ) for compound **3** collected under zero applied static field ($H_{dc} = 0 \text{ Oe}$; *top* and *middle*) and under an applied static field ($H_{dc} = 200 \text{ Oe}$; *bottom*). The red solid lines represent the best fit to Eqn. S2. The orange, teal, and purple lines are the individual components of the magnetization relaxation for Orbach, Raman, and QTM

processes, respectively. Parameters are summarized in Table S16. The error bars on the relaxation time have been calculated from the α -parameters of the generalized Debye fit with the log-normal distribution.¹⁸

Table S16. Magnetic relaxation parameters obtained from the fit of the temperature dependent relaxation times (Fig. S17 and S18) for compound **1** and **3**. Best fits were obtained with quantum tunneling of the magnetization, Orbach, and Raman contributions (Eqn. S1-S2).

		Compound 1 (Co ^{II})			Compound 3 (Fe ^I)		
H_{dc}		0 Oe		1400 Oe	0 Oe		200 Oe
Parameters		HF ^[a]	LF ^[b]		HF ^[a]	LF ^[b]	
QTM	τ_{QTM}	0.0012 s	0.117 s		0.0012 s	0.707 s	
Orbach	τ_0	1.96 x 10 ⁻⁵ s			1.83 x 10 ⁻⁴ s		1.03 x 10 ⁻¹⁰ s
	U_{eff}	18.5 K (12.8 cm ⁻¹)			18.7 K (12.9 cm ⁻¹)		334 K (232 cm ⁻¹)
Raman	C	6.63 x 10 ⁻⁵ s ⁻¹ K ⁻ⁿ	1.82 x 10 ⁻² s ⁻¹ K ⁻ⁿ	1.31 x 10 ⁻³ s ⁻¹ K ⁻ⁿ		1.27 x 10 ⁻⁴ s ⁻¹ K ⁻ⁿ	5.04 x 10 ⁻⁵ s ⁻¹ K ⁻ⁿ
	n	7.87	5.31	5.29		5.96	4.97
Direct	A						

[a] Fit parameters obtained from the high frequency (HF) region of the ac susceptibility. [b] Fit parameters obtained from the low frequency (LF) region of the ac susceptibility.

$$\text{Eqn. S1} \quad \tau^{-1} = \tau_{Orbach}^{-1} + \tau_{Raman}^{-1} + \tau_{Direct}^{-1} + \tau_{QTM}^{-1}$$

$$\text{Eqn. S2} \quad \tau^{-1} = \tau_0^{-1} \exp\left(-\frac{U_{eff}}{k_B T}\right) + CT^n + AH^4T + \frac{B_1}{1 + B_2 H^2}$$

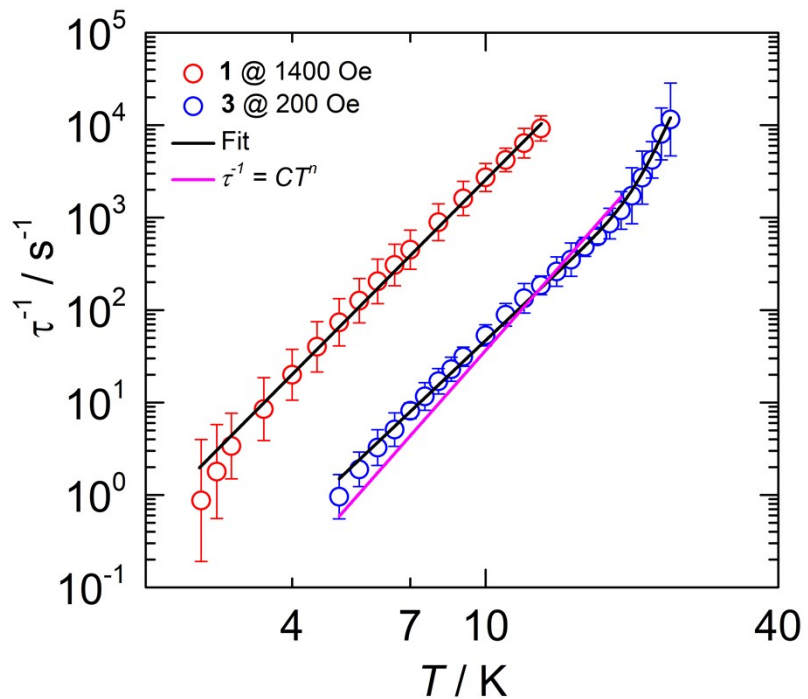


Fig. S18. Temperature dependence of the relaxation times (τ) in the presence of an applied static field for **1** (red) and **3** (blue). The estimated standard deviations of the relaxation times were calculated from the α parameters of the generalized Debye fits and the log-normal distribution.^[25] The solid black line represents the best fit to Eqn. S2. The solid pink line represented the Raman parameters ($C = 1.27 \times 10^{-4} \text{ s}^{-1} \text{ K}^{-n}$, $n = 5.96$) from the fit of the relaxation times obtained at zero field ($H_{dc} = 0 \text{ Oe}$), which fall within the standard deviations.

Magnetic Circular Dichroism (MCD) Measurements

MCD measurements were recorded on a Jasco J-1700 CD spectrometer and an Oxford SpectromagPT cryogen free magneto-optical superconducting magnet system. MCD spectra were recorded on mulls prepared in an inert atmosphere, of the solid compounds in Parabar 10312 oil from Hampton Research, sandwiched between quartz slides. The spectrum without any applied field was used as the background for the measurements.

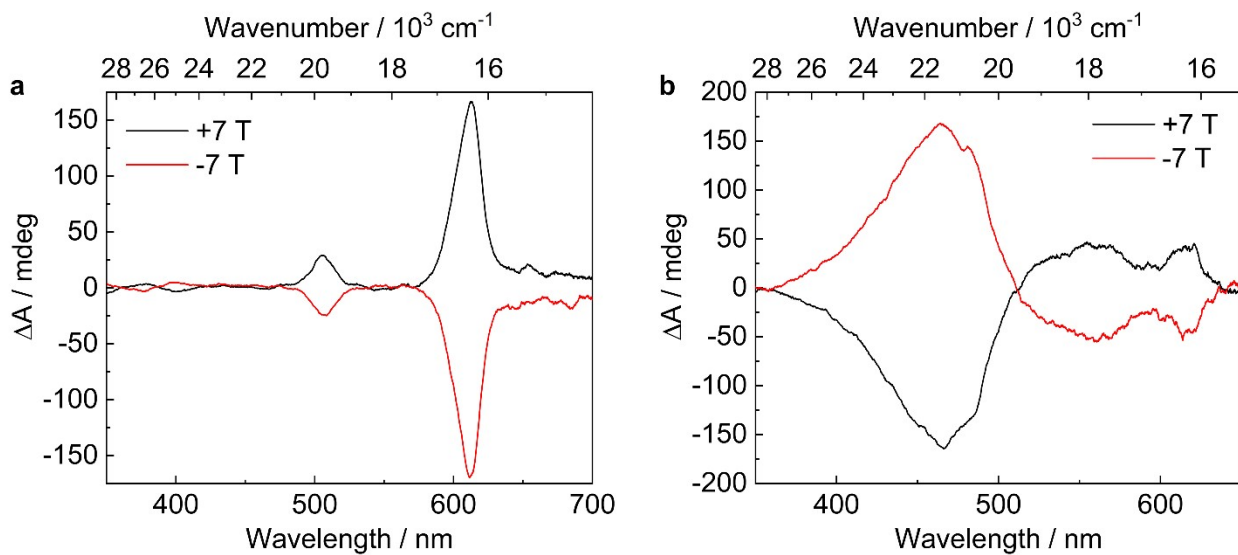


Fig. S19. MCD spectra for (a) **3** and (b) **1** obtained at 1.55 K with applied magnet field of +7 (black line) and -7 T (red line).

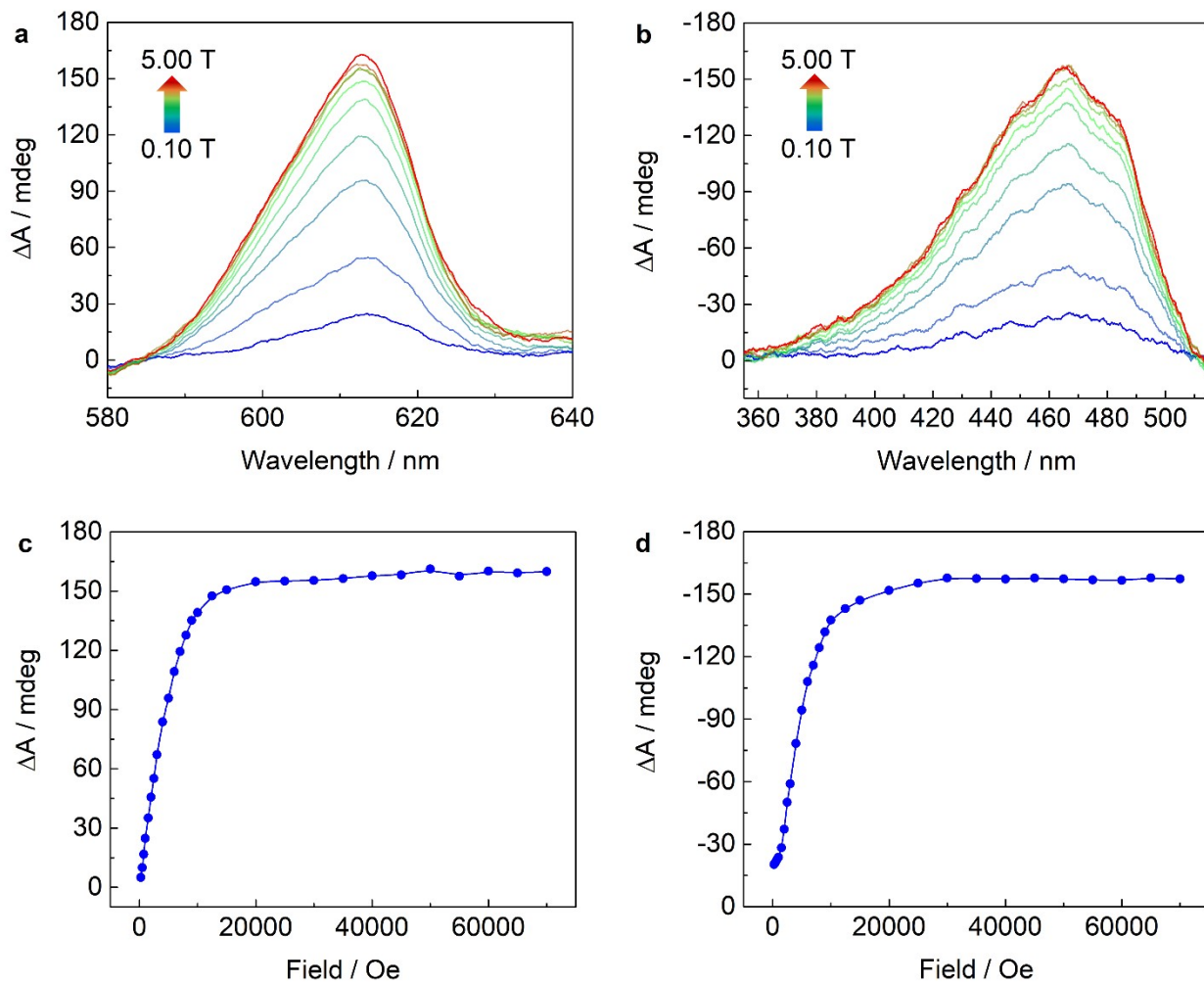


Fig. S20. Field dependence of the electronic transition centered at (a) 465 nm for **3** and (b) 613 nm for **1** obtained at 1.55 K. (c) and (d) Magnetization plot for the transitions.

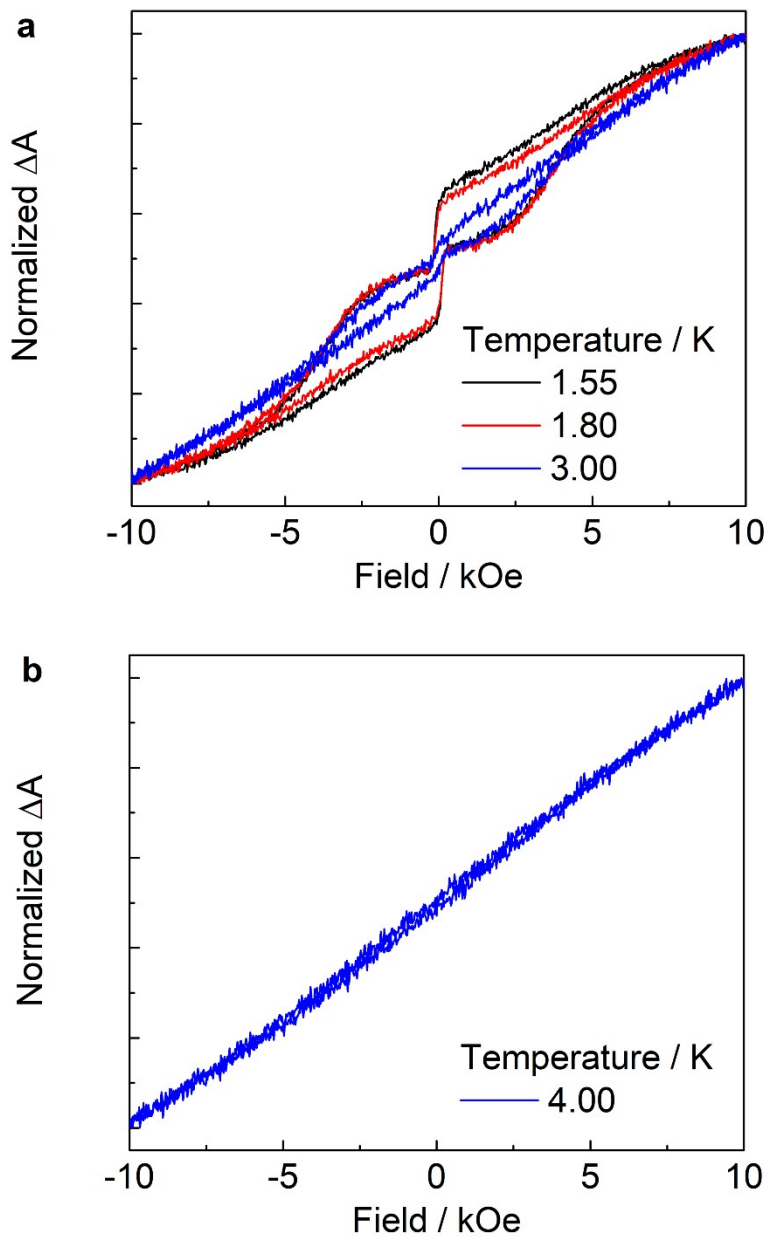


Fig. S21. Magneto-optical hysteresis data collected on MCD spectrometer for the transition centered at 465 nm (**3**) at (a) indicated temperatures and (b) 4 K. A sweep rate of 19 Oe s^{-1} was used.

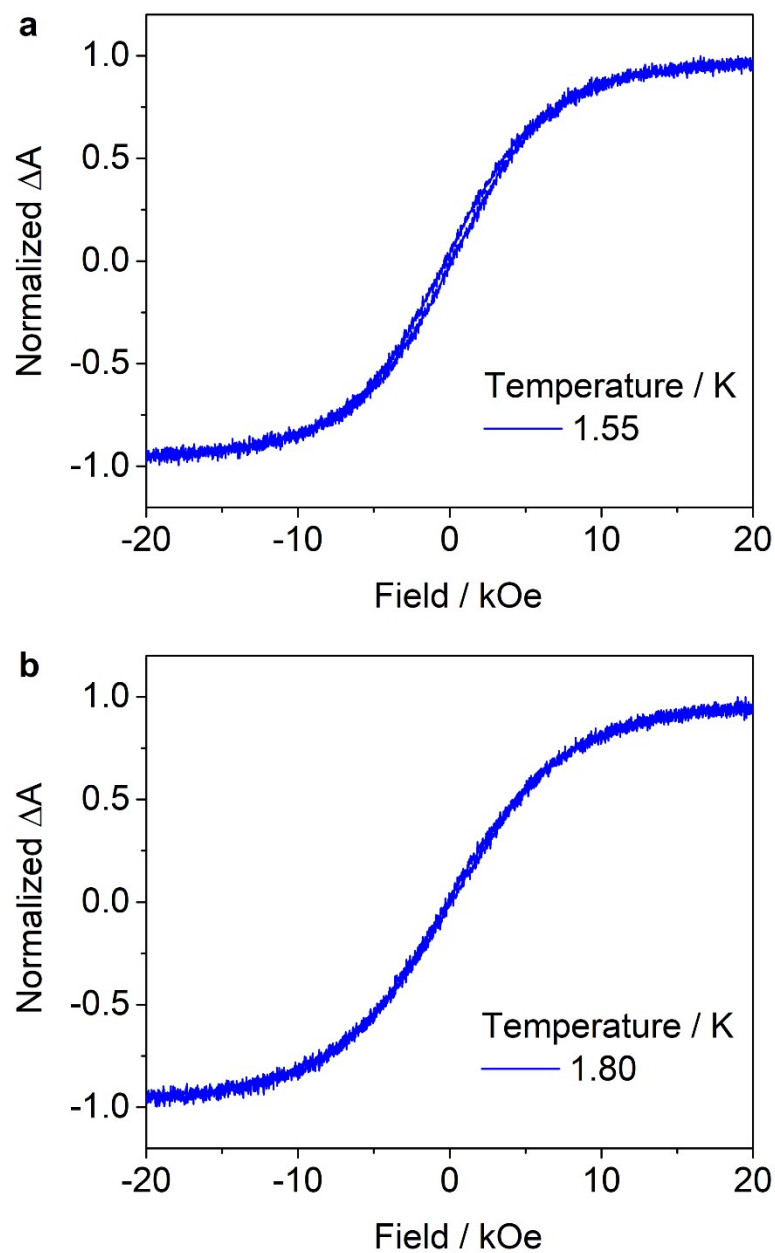


Fig. S22. Magneto-optical hysteresis data collected on MCD spectrometer for the transition centered at 613 nm (**1**) obtained at (a) 1.55 K and (b) 1.8 K. A sweep rate of 19 Oe s⁻¹ was used.

Supplementary References

- [1] A. Torvisco, K. Decker, F. Uhlig, K. Ruhlandt-Senge. *Inorg. Chem.* **2009**, *48* (23), 11459–11465.
- [2] R. A. Bartlett, P. Power. *J. Am. Chem. Soc.* **1987**, *109* (24), 7563–7564.
- [3] G. M. Sheldrick. *Acta Crystallogr. Sect. Found. Adv.* **2015**, *71* (1), 3–8.
- [4] G. M. Sheldrick. *Acta Crystallogr. Sect. C Struct. Chem.* **2015**, *71* (1), 3–8
- [5] a) B. O. Roos in *Advances in Chemical Physics, Ab Initio Methods in Quantum Chemistry II*, Vol. 69 (Ed.: K. P. Lawley), Wiley, New York, **1987**, pp. 399–455; b) P. Siegbahn, A. Heiberg, B. Roos, B. Levy. *Phys. Scripta*, **1980**, *21*, 323–327; c) B. O. Roos, P. R. Taylor, P. E. M. Siegbahn. *Chem. Phys.*, **1980**, *48*, 157–173; d) P. E. M. Siegbahn, J. Almlöf, A. Heiberg, B. Roos. *J. Chem. Phys.*, **1981**, *74*, 2384–2396.
- [6] a) C. Angeli, R. Cimiraglia, S. Evangelisti, T. Leininger, J.-P. Malrieu. *J. Chem. Phys.* **2001**, *114*, 10252–10264; b) C. Angeli, R. Cimiraglia, J.-P. Malrieu. *Chem. Phys. Lett.* **2001**, *350*, 297–305; c) C. Angeli, R. Cimiraglia, J.-P. Malrieu. *J. Chem. Phys.* **2002**, *117*, 9138–9153.
- [7] a) S. K. Singh, J. Eng, M. Atanasov, F. Neese. *Coord. Chem. Rev.* **2017**, *344*, 2–25; b) M. Atanasov, D. Ganyushin, K. Sivalingam, F. Neese in *Molecular Electronic Structures of Transition Metal Complexes II* (Eds.: D. M. P. Mingos, P. Day, J. P. Dahl), Springer, Berlin, **2012**, pp. 149–220.
- [8] Gaussian 09, Revision E.01, M. J. Frisch, G. W. Trucks, H. B. Schlegel, G. E. Scuseria, M. A. Robb, J. R. Cheeseman, G. Scalmani, V. Barone, G. A. Petersson, H. Nakatsuji, X. Li, M. Caricato, A. Marenich, J. Bloino, B. G. Janesko, R. Gomperts, B. Mennucci, H. P. Hratchian, J. V. Ortiz, A. F. Izmaylov, J. L. Sonnenberg, D. Williams-Young, F. Ding, F. Lipparini, F. Egidi, J. Goings, B. Peng, A. Petrone, T. Henderson, D. Ranasinghe, V. G. Zakrzewski, J. Gao, N. Rega, G. Zheng, W. Liang, M. Hada, M. Ehara, K. Toyota, R. Fukuda, J. Hasegawa, M. Ishida, T. Nakajima, Y. Honda, O. Kitao, H. Nakai, T. Vreven, K. Throssell, J. A. Montgomery, Jr., J. E. Peralta, F. Ogliaro, M. Bearpark, J. J. Heyd, E. Brothers, K. N. Kudin, V. N. Staroverov, T. Keith, R. Kobayashi, J. Normand, K. Raghavachari, A. Rendell, J. C. Burant, S. S. Iyengar, J. Tomasi, M. Cossi, J. M. Millam, M. Klene, C. Adamo, R. Cammi, J. W. Ochterski, R. L. Martin, K. Morokuma, O. Farkas, J. B. Foresman, and D. J. Fox, Gaussian, Inc., Wallingford CT, **2009**.
- [9] a) J. P. Perdew, K. Burke, M. Ernzerhof. *Phys. Rev. Lett.*, **1996**, *77*, 3865–3868; b) J. P. Perdew, K. Burke, M. Ernzerhof. *Phys. Rev. Lett.*, **1996**, *78*, 1396.
- [10] a) M. Ernzerhof, G. E. Scuseria. *J. Chem. Phys.* **1999**, *119*, 5029–5036; b) C. Adamo, V. Barone. *J. Chem. Phys.* **1999**, *110*, 6158–6170.
- [11] a) A. Schäfer, H. Horn, R. Ahlrichs. *J. Chem. Phys.* **1992**, *97*, 2571–2577; b) F. Weigend, R. Ahlrichs. *Phys. Chem. Chem. Phys.* **2005**, *7*, 3297–3305.
- [12] a) *ADF2019*. SCM, Theoretical Chemistry, Vrije Universiteit Amsterdam, The Netherlands. <http://www.scm.com>. 2019; b) G. te Velde, F. M. Bickelhaupt, E. J. Baerendes, C. Fonseca Guerra,

S. J. A. Gisbergen, J. G. Snijders, T. Ziegler. *J. Comp. Chem.* **2001**, *22*, 931–967; c) C. Fonseca Guerra, J. G. Snijders, G. te Velde, E. J. Baerends. *Theor. Chem. Acc.* **1998**, *99*, 391–403.

[13] a) E. van Lenthe, E. J. Baerends, J. G. Snijders. *J. Chem. Phys.* **1993**, *99*, 4597–4610; b) E. van Lenthe, E. J. Baerends, J. G. Snijders. *J. Chem. Phys.* **1994**, *101*, 9783–9792; c) E. van Lenthe, R. van Leeuwen, E. J. Baerends, J. G. Snijders. *Int. J. Quantum. Chem.* **1996**, *57*, 281–293.

[14] E. van Lenthe, E. J. Baerends. *J. Comp. Chem.* **2003**, *24*, 1142–1156.

[15] a) F. Neese. *WIREs Comput. Mol. Sci.* **2017**, *8*, e1327; b) F. Neese, F. Wennmohs, U. Becker, C. Ripplinger. *J. Chem. Phys.* **2020**, *152*, 224108.

[16] a) B. O. Roos in *Advances in Chemical Physics, Ab Initio Methods in Quantum Chemistry II*, Vol. 69 (Ed.: K. P. Lawley), Wiley, New York, **1987**, pp. 399–455; b) P. Siegbahn, A. Heiberg, B. Roos, B. Levy. *Phys. Scripta*, **1980**, *21*, 323–327; c) B. O. Roos, P. R. Taylor, P. E. M. Siegbahn. *Chem. Phys.*, **1980**, *48*, 157–173; d) P. E. M. Siegbahn, J. Almlöf, A. Heiberg, B. Roos. *J. Chem. Phys.*, **1981**, *74*, 2384–2396; e) B. O. Roos, R. Lindh, P. Å. Malmqvist, V. Veryazov, P.-O. Widmark. *Multiconfigurational Quantum Chemistry*. Wiley, Hoboken, NJ, **2016**.

[17] a) C. Angeli, R. Cimiraglia, S. Evangelisti, T. Leininger, J.-P. Malrieu. *J. Chem. Phys.* **2001**, *114*, 10252–10264; b) C. Angeli, R. Cimiraglia, J.-P. Malrieu. *Chem. Phys. Lett.* **2001**, *350*, 297–305; c) C. Angeli, R. Cimiraglia, J.-P. Malrieu. *J. Chem. Phys.* **2002**, *117*, 9138–9153.

[18] a) M. Douglas, N. M. Kroll. *Ann. Phys.* **1974**, *82*, 89–155; b) B. A. Heß. *Phys. Rev. A*, **1986**, *33*, 3742–3748.

[19] a) F. Neese, T. Petrenko, D. Ganyushin, G. Olbrich. *Coord. Chem. Rev.* **2007**, *251*, 288–327; b) M. Atanasov, D. Aravena, E. Suturina, E. Bill, D. Maganas, F. Neese. *Coord. Chem. Rev.* **2015**, *289–290*, 177–214.

[20] a) F. Neese. *J. Chem. Phys.* **2005**, *122*, 034107; b) A. Berning, M. Shcwizer, H.-J. Werne, P. J. Knowles, P. Palmieri. *Mol. Phys.* **2000**, *98*, 1823–1833; c) B. A. Heß, C. M. Marian, U. W. Wahlgren, O. Gropen. *Chem. Phys. Lett.* **1996**, *251*, 365–371.

[21] a) D. A. Pantazis, X.-Y. Chen, C. R. Landis, F. Neese. *J. Chem. Theory Comput.* **2008**, *4*, 908–919; b) F. Weigend, R. Ahlrichs. *Phys. Chem. Chem. Phys.* **2005**, *7*, 3297–3305.

[22] G. L. Stoychev, A. A. Auer, F. Neese. *J. Chem. Theory Comput.* **2017**, *13*, 554–562.

[23] a) M. Atanasov, D. Ganyushin, K. Sivalingam, F. Neese. *A Modern First-Principles View of Ligand Field Theory Through the Eyes of Correlated Multireference Wavefunctions in Molecular Electronic Structure of Transition Metal Complexes*. Eds. D. M. P. Mings, P. Day, J. P. Dahl. Springer, Berlin, Germany, **2012**; b) S. K. Singh, J. Eng, M. Atanasov, F. Neese. *Coord. Chem. Rev.* **2017**, *344*, 2–25.

[24] S. K. Singh, M. Atanasov, F. Neese, *J. Chem. Theory Comput.* **2018**, *14*, 4662–4677.

[25] D. Reta, N. F. Chilton, *Phys. Chem. Chem. Phys.*, **2019**, *21*, 23567–23575.